CIAMTIS

U.S. DOT Region 3 University Transportation Center

Passive Strain Sensing for Structural Health Monitoring Using Retroreflective Sheeting Materials

October 25, 2022

Prepared by:
H. Power and H. Shenton III
University of Delaware

r3utc.psu.edu

PennState
College of Engineering

LARSON TRANSPORTATION INSTITUTE

DISCLAIMER

The contents of this report reflect the views of the authors, who are responsible for the facts and the accuracy of the information presented herein. This document is disseminated in the interest of information exchange. The report is funded, partially or entirely, by a grant from the U.S. Department of Transportation's University Transportation Centers Program. However, the U.S. Government assumes no liability for the contents or use thereof.

1. Report No. CIAM-UTC-REG18	**2. Government Accession No.**	**3. Recipient's Catalog No.**
4. Title and Subtitle Passive Strain Sensing for Structural Health Monitoring Using Retroreflective Sheeting Materials	**5. Report Date** October 25, 2022	
	6. Performing Organization Code	
7. Author(s) H. Power and H. Shenton III	**8. Performing Organization Report No.**	
9. Performing Organization Name and Address Department of Civil and Environmental Engineering University of Delaware DuPont Hall, 127 The Green Newark, DE 19716	**10. Work Unit No. (TRAIS)**	
	11. Contract or Grant No. 69A3551847103	
12. Sponsoring Agency Name and Address U.S. Department of Transportation Research and Innovative Technology Administration 3rd Fl, East Bldg E33-461 1200 New Jersey Ave, SE Washington, DC 20590	**13. Type of Report and Period Covered** Final Report 2/2020 - 1/20/22	
	14. Sponsoring Agency Code	

16. Abstract

Retroreflective sheeting materials (RRSM) are used for various applications in engineering, but primarily for traffic signs and pavement markings. There are several ASTM standard types of RRSM that have required values of retroreflection to ensure safe usage. Retroreflectivity is the portion of light returned to the light source measured in candelas per lux per square meter, as measured using a retroreflectometer. It is theorized that as load is applied to RRSM, the retroreflection will change and have a reasonably linear relationship to the material's strain (ε), thus opening the possibility for using RRSM material as a passive strain sensor for structural health monitoring that is low cost, practical, and innovative. A total of 10 materials, manufactured by Avery Dennison and 3M, were loaded in tension and their strain and retroreflectivity were measured at 4.45-N and 8.90-N (1-lb and 2-lb) load intervals. Specimens were subjected to three loading and unloading cycles, and their sensitivity (retroreflectivity divided by strain) was calculated to determine their feasibility for use as passive strain sensors. Results show that the retroreflectivity of RRSM does change when subjected to load, and that certain materials demonstrate a reasonably linear relation to strain. Furthermore, others do not return to their baseline retroreflectivity but degrade through the course of repeated loading. The 10 materials were also subjected to strength tests to determine their failure stresses and strain to failure. Four of the materials have the highest retroreflective sensitivity to strain, have high failure stresses and strains, and are the most likely to perform well as passive strain sensors. These four materials were subjected to microscopic evaluation of their reflecting layer to determine why retroreflectivity changes with applied load. Additionally, initial environmental exposure tests were performed on one material type to determine best methods of adhering RRSM to common substrates and to evaluate how retroreflectivity changes with extended exposure. Future research will include continued testing of RRSMs to better understand their potential use as passive strain sensors.

17. Key Words Retroreflective sheeting materials, traffic signs, pavement markings, structural health monitoring, stress, passive strain, retroreflectivity	**18. Distribution Statement** No restrictions. This document is available from the National Technical Information Service, Springfield, VA 22161		
19. Security Classif. (of this report) Unclassified	**20. Security Classif. (of this page)** Unclassified	**21. No. of Pages** 64	**22. Price**

Form DOT F 1700.7   **(8-72)   Reproduction of completed page authorized**

Table of Contents

List of Tables

r3utc.psu.edu

List of Figures

Introduction

BACKGROUND AND MOTIVATION

Civil infrastructure provides functionality to a society through facilities like buildings, bridges, highways, factories, and so on. These infrastructure systems degrade with age, natural disasters, and extreme loading events, and need to be maintained and repaired to ensure safe and effective use [1-3]. Current infrastructure management methods rely primarily on qualitative visual inspections. These inspections do not tell owners about issues that cannot be seen by eye, are labor intensive, and are susceptible to error, so more quantitative methods of inspection may be necessary [4, 5]. Structural health monitoring (SHM) is the implementation of devices on a structure that detect changes and allow engineers to evaluate condition in a non-destructive, quantitative manner to provide appropriate maintenance and repairs [6]. SHM systems consist of sensing networks and data collection that provide knowledge in early stages of problems so that appropriate decisions can be made to reduce maintenance and repair costs and extend the lives of structures [3].

Strain measurements are commonly used to evaluate the health of a structure. Strain relates directly to local damage and is one of the most important parameters to judge the health of a structure [7, 8]. Strain measurements tell engineers about typical wear due to cyclic loading that cause material fatigue, and also about damage caused by excessive loading events from impact or natural disasters. While conventional wired "active" gages have high sensitivity, their downsides are the need for power, excessive cabling, connectivity challenges, dedicated data acquisition, and cost [6, 9]. Due to this, there is a growing need to develop passive strain gauges for structural health monitoring. While passive strain gauges negate the need for power and wiring, they are often not as sensitive or as accurate as active strain gauges.

SHM does not just refer to civil infrastructure, but also to mechanical systems, medical applications, aerospace structures, and so on. In all of these industries, strain sensing is used to evaluate performance and improve safety. Mechanical systems can experience high levels of vibration and excessive loading, and strain sensing indicates any deformations experienced [9]. In medical applications, strain sensors can be implanted to monitor bone fractures [10] and to monitor orthopedic implants during exercises to prevent failure due to repetitive loading [11]. The aerospace industry uses strain gauges to determine fatigue on systems subjected to cyclic loading and determine when they have reached their useable life [12]. Each of these applications benefits from the use of passive strain sensors over active sensors because they tend to be lighter, have longer life spans, and allow for more effective infrastructure management [9, 13].

In civil infrastructure, particularly bridges, SHM is beneficial because it allows for changes in stress due to damage, fatigue, and deterioration to be readily detected to ensure safety and avoid catastrophic failure. Bridges are typically designed to have 50 to 100 years of service life, but as they age, they deteriorate due to the environment and traffic loads they experience. Bridges can also experience excessive loading events like impact, collision, and earthquake loading [7]. All these loading scenarios influence the safety of bridges, so they need to be monitored and maintained to ensure safety [14]. A number of case studies have been performed on SHM systems implemented on bridges such as the Golden Gate Bridge in California [15], the Indian River Inlet Bridge in Delaware [16], the Jiubao Bridge in China [17], and the Sungsu Bridge

in Korea [18]. Each of these systems is unique, but their common goal is to monitor the bridge via strain and other measurements to evaluate performance.

Strain sensing is a widely researched topic, especially in structural health monitoring. Active sensors, which require power and wiring, are commonly used, as well as semi-active sensors, which are wireless but require power [19, 20]. Passive sensors are ones that require neither power nor wiring. Traditional strain gauges are active, such as bonded resistive gauges, vibrating wires, and fiber optic sensors, and they require constant power and data collection, making them not well suited for long-term monitoring [21]. Using passive strain sensors, rather than active sensors, is preferred because they are simpler to install and maintain and the data collected are easier to manage, making their long-term usage more viable. [5, 6, 22, 23]. Various types of passive strain sensors have been developed, such as radio frequency identification (RFID) sensors, which can be used in various industries because in addition to measuring strain, they also have the ability to quantify temperature and humidity changes, making them useful in medical applications [19, 24-26]. Laser speckle strain gauges are a wireless means to measure displacement by tracking how speckles on the surface of a structure move when load is applied [27]. Tan et al. developed a passive strain sensor using magnetic elements separated by a deformable layer that changed dimensions as it was loaded, altering the distance between the magnetic layers and the harmonic field, so that strain could be measured [28]. Inductance capacitators (IC) can also be made to be passive to sense both temperature and strain, which has been observed to be useful in various mechanical systems where there are many structural elements that experience frequent high-speed rotations [29]. Each of these unique passive strain sensing devices has its shortcomings, including complexity, expensive fabrication and software, and extensive wireless sensor networks, so there is a continued desire to produce novel passive strain sensors. This report presents a novel passive strain sensor for SHM using retroreflective sheeting materials to measure strain in infrastructure.

OBJECTIVES OF THE RESEARCH

This research aims to accomplish four main objectives:
- Develop an understanding of how retroreflective sheeting materials (RRSMs) respond to applied load within the context of its use as a passive strain sensor.
- Determine how RRSM adhere to common structural materials.
- Characterize degradation of RRSMs to environmental exposure.
- Determine the fundamental mechanism by which the retroreflectivity of RRSM changes when it is strained.

OUTLINE OF THE REPORT

This report presents research conducted to determine the viability of using RRSM as a passive strain sensor for structural health monitoring. Chapter 1 presents the background, motivation, and objectives of this research. Chapter 2 introduces retroreflective sheeting materials and discusses their implementation as passive strain sensors. The methodology of tests performed during this research, including tension, strength, exposure, and microscopic evaluation tests, is presented in Chapter 3 along with an overview of the various types of RRSM that were analyzed. Chapter 4 presents the results of all tests performed, and in Chapter 5 the results are discussed and viability of the various types of RRSM are determined. Conclusions are presented in Chapter 6, and anticipated future work is discussed in Chapter 7.

Retroreflective Sheeting Materials and Their Potential Use as Sensors in Structural Health Monitoring

RETROREFLECTIVE SHEETING MATERIALS

Retroreflective sheeting materials are flexible reflective, fabric-like materials that are developed and used for various applications in engineering, primarily for traffic signs and pavement markings. ASTM D4956, "Standard Specification for Retroreflective Sheeting for Traffic Control" [30], defines standard specifications for 11 different types of sheeting material. They are produced by various companies, for example, 3M, Avery Dennison, and Nippon, to name a few. An innovative use of RRSM presented by Mauri et al. [31] includes their use as a building envelope coating that reflects sunlight to reduce effects of the urban heat island phenomena to reduce temperatures. Other research in retroreflective materials includes evaluation of in-service traffic signs and pavement markings to assess their durability and determine which factors contribute to degrading retroreflectivity such as GPS location, physical orientation, color, and environmental factors [32-34]. There is also interest in the development of new reflective materials to optimize their retroreflectivity and production technology [35, 36].

There are various types of standard RRSM, and they are produced using a range of technologies to ensure that roadway signs, markings and other reflective surfaces are clearly visible to individuals. RRSM consist of reflective elements made of either beads or prisms [37]. Glass beads are used in lower-grade materials, such as standardized Type I materials, and prisms are used in more efficient retroreflective materials, such as Type XI. Figure 1 shows a general cross section of an RRSM with a metallized glass bead reflecting layer, such as a Type I and of an RRSM with an unmetallized prismatic reflecting layer, such as a Type XI material.
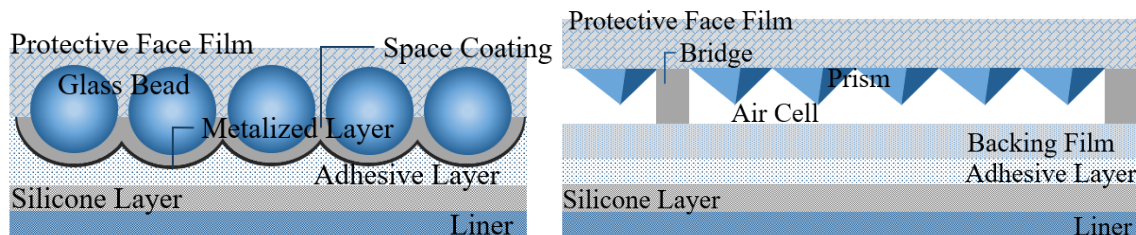
(a) Metallized glass bead RRSM   (b) Unmetallized prismatic RRSM

Figure 1. Material cross-sections.

The Federal Highway Administration (FHWA) Manual on Uniform Traffic Control Devices (MUTCD) [38] requires all public agencies to maintain minimum levels of sign retroreflectivity. To demonstrate

compliance, agencies can measure retroreflectivity using handheld sign retroreflectometers. Retroreflectometers produce a light beam when held against a material and a trigger is pulled. They then measure the amount of light returned to the device and display a reading of retroreflectivity. It is theorized that as load is applied to RRSM, the retroreflection will change in intensity and may have a reasonably linear relationship to the level of strain induced into the material. By knowing this relationship, RRSM may be used as an innovative, low cost, and practical way to passively monitor structures.

APPLICATIONS OF RRSM SENSORS IN STRUCTURAL HEALTH MONITORING

The authors have demonstrated, through tests and as reported herein, that as load is applied to a retroreflective sheeting material, the retroreflection changes in intensity. By correlating the change in retroreflectivity to the strain induced in the material, the RRSM may potentially be used as a passive strain sensor. It is envisioned that a sample or "target" of RRSM, after proper surface preparation, can be placed on a steel, aluminum, or concrete surface and an RR measurement taken of the target using a handheld retroreflectometer. At different intervals in time, or after significant events, a new reading can be taken and the result compared to the earlier "baseline" reading. Any change in the RR can be correlated to change in local strain at the target. There are several practical applications for using an RRSM as a sensor for structural health monitoring, such as:

- As a crack gage when the RRSM is placed across a crack in a concrete structure.
- To monitor strains/stresses in precast or prestressed concrete girders. For example, by measuring the change in retroreflectivity of an RRSM sample placed on a girder while it is continuously supported on the ground, compared to after it is placed in service, i.e., the dead load is imposed. Or, by measuring the change in retroreflectivity of an RRSM sample placed on a prestressed girder before the strands are cut, compared to after the strands are cut.
- To monitor the distribution of dead-load stresses in a structure. By placing RRSM sensors on various members of a structure and measuring the baseline retroreflectivity at one time, and comparing these readings to measurements taken at a later time, changes in the retroreflectivity could be an indication of a redistribution of dead-load stresses that could be an indication of possible damage in the structure.
- To monitor pseudo-live loads in a structure. Changes in strain in a bridge due to vehicle live loads are relatively small, requiring a very sensitive sensor to measure them. Changes in retroreflectivity of RRSM due to small strains may not be large enough to use it as a passive strain sensor for live-load monitoring, but this application can be explored provided high enough sensitivities are achieved.
- Finally, to monitor residual stresses in a structure. ASTM E837-20 [39,40] describes a procedure for measuring residual stresses in the surface of a material by drilling a hole in the center of a specially designed strain gage rosette. Perhaps this procedure could be adapted using RRSM sensors.

Many departments of transportation (DOTs) have access to and familiarity with retroreflectometers and RRSM, which will make their implementation as passive strain sensors simple and easy. The installation, strain measurement, and technology of these sensors are straightforward and inexpensive. The objective of this research has been to investigate, develop, and demonstrate that an innovative passive strain sensor can be made from RRSM for use in structural health monitoring.

IMPLEMENTING RRSM AS STRAIN SENSORS

This section illustrates, through a series of photos, how simple the process could be to deploy an RRSM strain sensor on a structure. The material used in this illustration is just one of many types that have been

CIAMTIS
U.S. DOT Region 3 University Transportation Center

tested and will be described in more detail in Chapter 3. This is not intended to be a comprehensive list of instructions of the process but does demonstrate the basic steps that would be required.

RRSMs are manufactured in large rolls, and the first step is to cut a section of material from the roll. Referring to Figure 2, use a template to trace a "dog bone" shape sensor onto the material. A "dog bone" shape is used so that strain concentrates along the center of the specimen, within their gauge length, and to provide larger areas for bonding at the ends of the sensor for better adhesion to the substrate. Measuring "dog bone" shape RRSM sensors retroreflectivity within their gauge length will ensure accurate readings and evaluation of the structure.
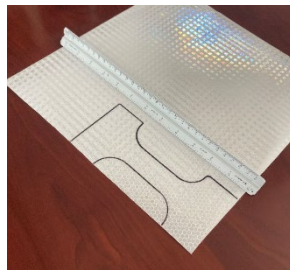
(a) RRSM and sensor template

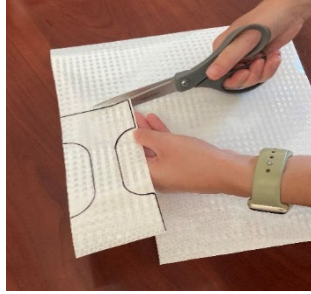(b) RRSM with "dog bone" sensor template placed for tracing

(c) Trace template onto RRSM

(d) Sensor traced onto RRSM

Figure 2. Step 1: Create strain sensor using RRSM, template the material

After the template is traced onto the RRSM, cut out the "dog bone" shape by first cutting a rectangle and then trimming the remaining excess, as seen in Figure 3.

(a) Cut a rectangle of RRSM around the sensor template

(b) Trim Excess RRSM so that the sensor is a "dog bone" shape

(c) Final RRSM sensor shape

Figure 3. Step 2: Cut a "dog bone" shape sensor from the RRSM

Once the RRSM sensor has been cut to the appropriate shape, shade the ends of the sensor with markers to ensure that retroreflective readings are only taken within the gauge length of the sensor, as shown in Figure 4.
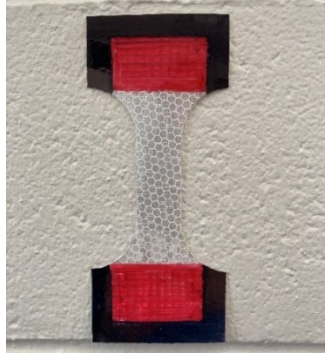
Figure 4. Step 3: Shade the ends of the sensor

Once the sensor has been prepared, the surface of the substrate must be prepared for proper adhesion. First, clean the surface of all debris and then wire brush the surface by hand. Next, clean the surface with a brush and acetone, as shown in Figure 5.

(a) Wire brush the surface of the substrate.

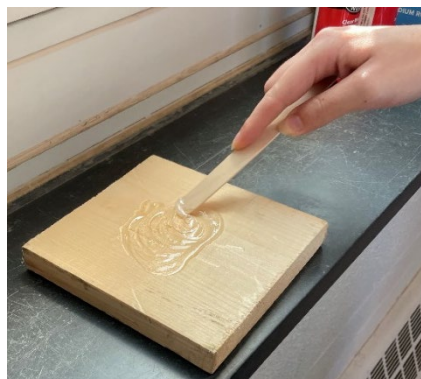(b) Brush debris from the surface of the substrate.

CIAMTIS
U.S. DOT Region 3 University Transportation Center

(c) Clean the substrate surface with acetone.

Figure 5. Step 4: Clean the surface of the substrate

For concrete structures, apply an epoxy coating to the substrate prior to adhesion and allow it to cure. For steel surfaces, sand the surface by hand after wire brushing. Figure 6 shows the epoxy application to a concrete substrate.

(a) Epoxy materials used to adhere sensor to concrete substrate.

(b) Mix 2-part epoxy prior to application.

CIAMTIS
U.S. DOT Region 3 University Transportation Center

(c) Skim coat the surface of the substrate with epoxy.

Figure 6. Step 5: Prepare the surface of the substrate.

After the substrate is prepared, remove the backing film from the sensor and adhere it to the structure. To ensure good adhesion, use a rubber roller on the sensor, using a barrier between the retroreflective surface and the roller, as seen in Figure 7.


(a) Remove backing film from RRSM and apply sensor to epoxy-coated substrate.

(b) Using a rubber roller, roll over the sensor to ensure adhesion.

Figure 7. Step 6: Adhere the sensor to the substrate.

When the sensor has been adhered to the structure, take initial retroreflective readings using a handheld sign reflectometer, as shown in Figure 8.

CI▲MTIS
U.S. DOT Region 3 University Transportation Center
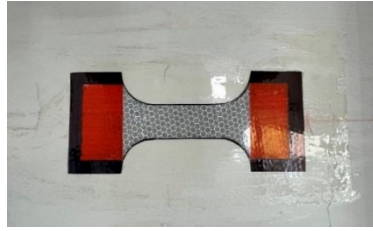
(a) RRSM sensor mounted to surface.

(b) Take retroreflective readings of the installed sensor.

Figure 8. Step 7: Take initial retroreflective readings of the sensor.

CHAPTER 3

Test Procedure

Presented in this chapter are the RRSM materials evaluated for their potential use as passive strain sensors as well as the test setups and procedures for tension, strength, exposure, and microscopic tests of those materials. Each of these materials is standardized by ASTM based on its reflecting elements and efficiency. Retroreflectivity for each of the materials presented in this chapter was measured using a handheld sign retroreflectometer, which is also introduced in this chapter. The baseline retroreflective variability for each of the materials tested was determined to ensure that changes in retroreflective readings can be attributed to load induced in the materials or environmental exposure.

MATERIALS TESTED

> Note: two manufacturers' materials were tested as part of this research study. The use of these two manufacturers materials is not an endorsement by the authors of either manufacturer's products for use in highway signs or the stated use by the manufacturer. There are other manufacturers of RRSM, but testing all manufacturers' materials was beyond the scope and budget of this project.

Three samples of 10 different materials were loaded in tension to determine the relationship between the material strain and retroreflectivity. Two manufacturers' materials were tested: Avery Dennison and 3M, and five different types of RRSM from each manufacturer were tested.

Material descriptions and photos of the 10 materials are presented in Table 1.

Table 1. Retroreflective sheeting materials tested.

Manufacturer	ASTM Type	Color	Designation	Photo
3M	I	White	3MTI	
3M	IV	White	3MTIV	
3M	VIII	Orange	3MTVIII	
3M	XI	White	3MTXIW	
3M	XI	Yellow	3MTXIY	
Avery Dennison	I	White	ADTI	
Avery Dennison	IV	White	ADTIV	
Avery Dennison	VIII	White	ADTVIII	
Avery Dennison	XI	White	ADTXIW	
Avery Dennison	XI	Yellow	ADTXIY	

As mentioned previously, ASTM D4956 defines standard specifications for 11 different types of sheeting material. Type I materials are engineering grade, typically consisting of glass beads, and are regarded as the lowest-quality RRSM, as they are the least reflective of all the types. Type IV retroreflective sheeting is high-intensity prismatic and made of unmetallized micoprismatic retroreflective-element material. Type VIII consists of unmetallized cube-corner micoprismatic retroreflective-element material [37] and are classified as super-high-intensity prismatic by 3M [41] and as maximum visual performance series prismatic by Avery Dennison [37]. Type XI materials are also made of unmetallized cube-corner micoprismatic retroreflective-element material [37]. 3M designates Type XI materials as super-high-efficiency sheeting, known as diamond grade (DG3) sheeting. DG3 sheeting is designed to reflect approximately twice the amount of light back to the source as high-intensity prismatic sheeting [41]. Avery Dennison classifies Type XI materials as OmniCube full-cube micoprismatic sheeting, and it is
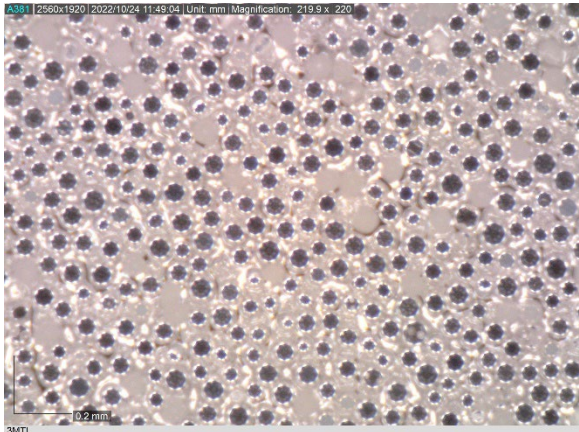
designed to reflect approximately 60% of the available light back to the source [37]. Photos of each material used in this research were taken using a DinoLite handheld microscope at 25, 100, and 220 times magnification, which are presented in Figures 9–18.
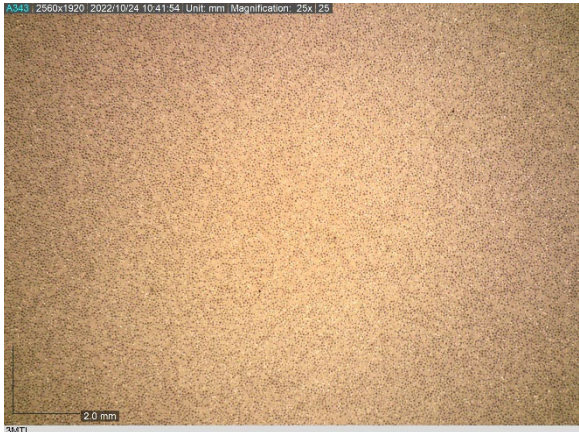
(a) 25 times magnification
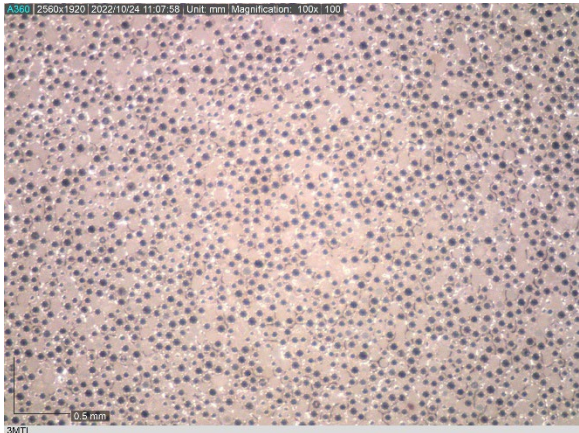
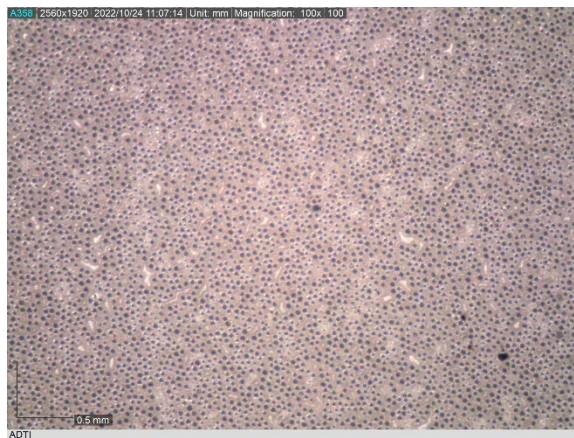(b) 100 times magnification

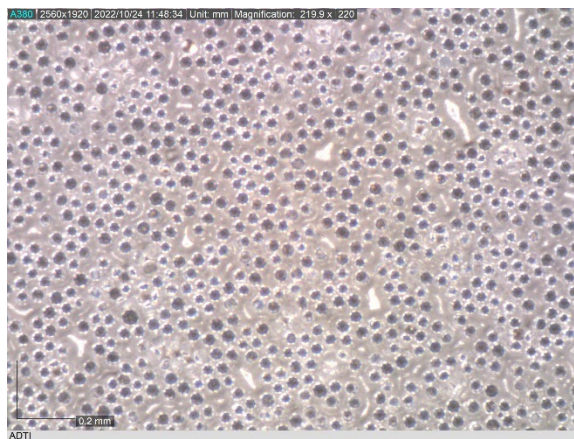(c) 220 times magnification

Figure 9. 3MTI material photos.

(a) 25 times magnification

(b) 100 times magnification

(c) 220 times magnification

Figure 10. ADTI material photos.

CIAMTIS
U.S. DOT Region 3 University Transportation Center

(a) 25 times magnification

(b) 100 times magnification

(c) 220 times magnification

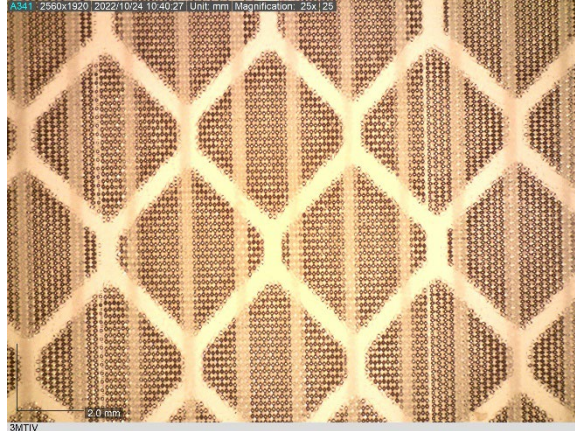**Figure 11. 3MTIV material photos.**

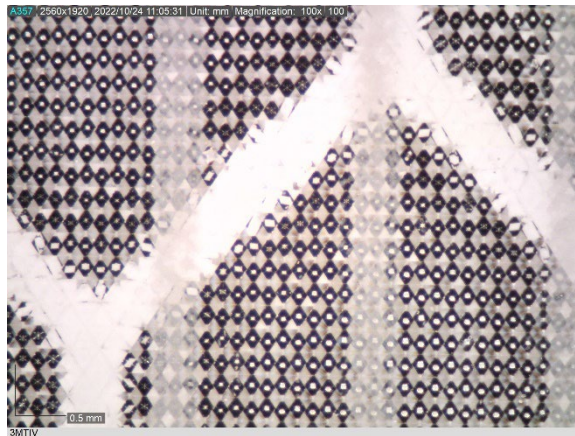(a) 25 times magnification

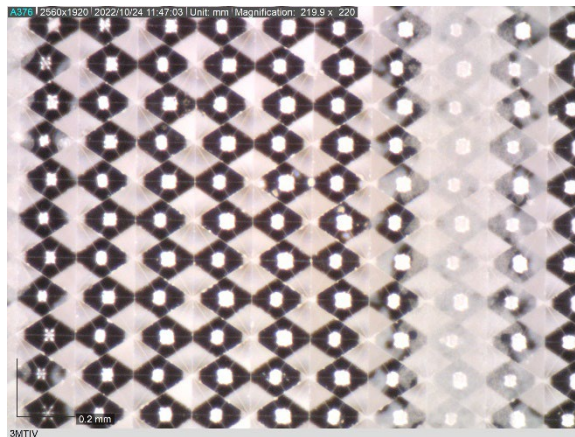(b) 100 times magnification

(c) 220 times magnification

Figure 12. ADTIV material photos.
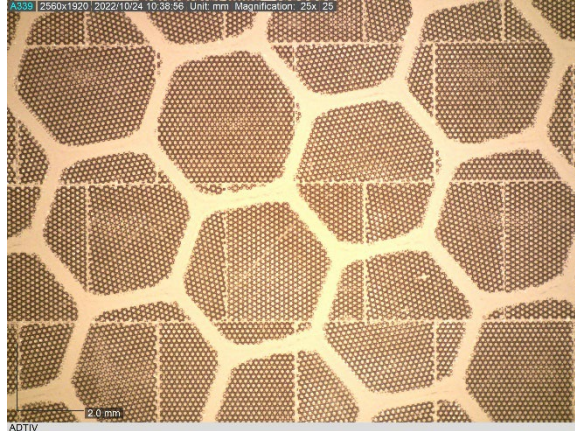
(a) 25 times magnification

(b) 100 times magnification

(c) 220 times magnification

Figure 13. 3MTVIII material photos.

(a) 25 times magnification

(b) 100 times magnification

(c) 220 times magnification

Figure 14. ADTVIII material photos.

(a) 25 times magnification
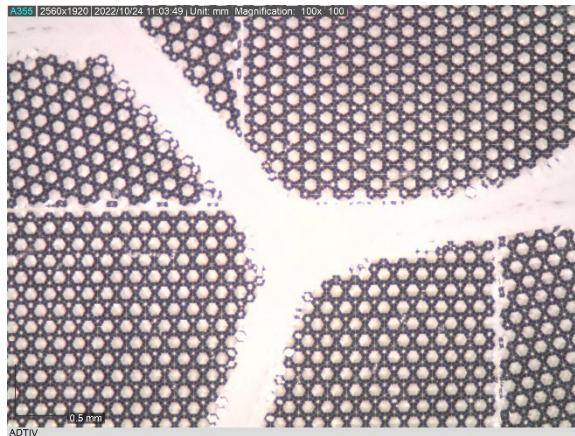

(b) 100 times magnification

(c) 220 times magnification

Figure 15. 3MTXIW material photos.

(a) 25 times magnification
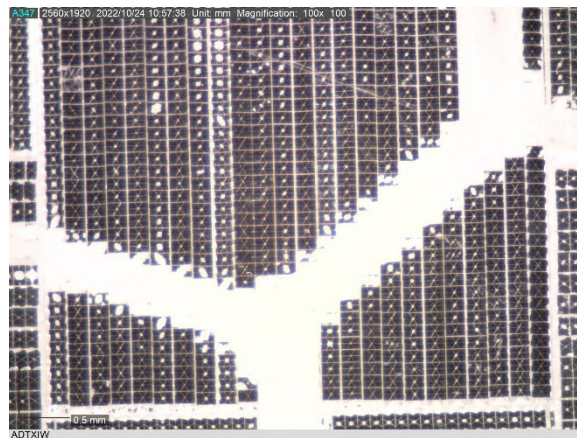
(b) 100 times magnification
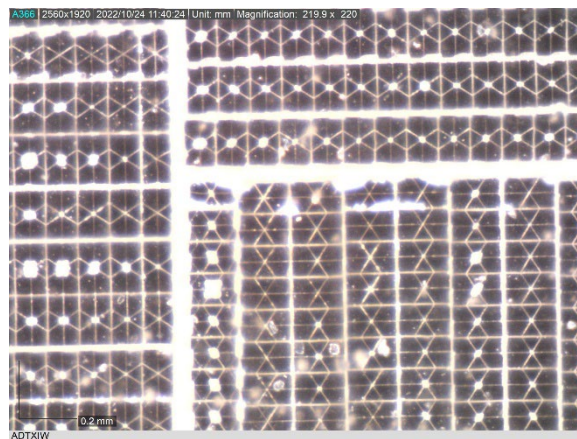
(c) 220 times magnification

Figure 16. ADTXIW material photos.
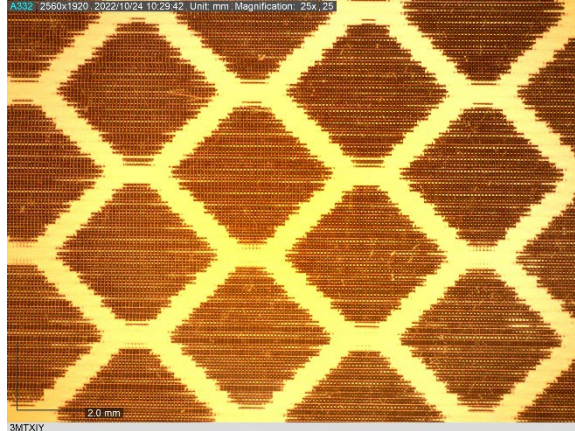
(a) 25 times magnification
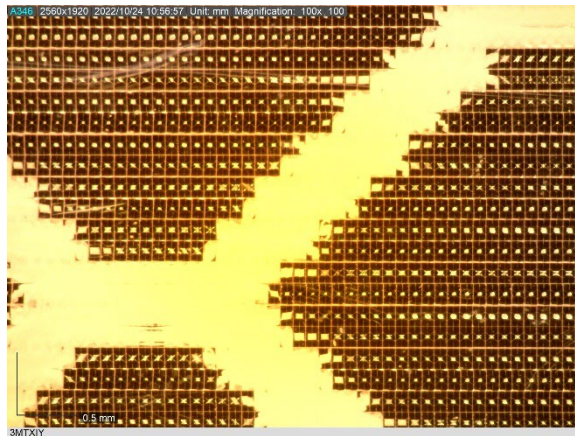
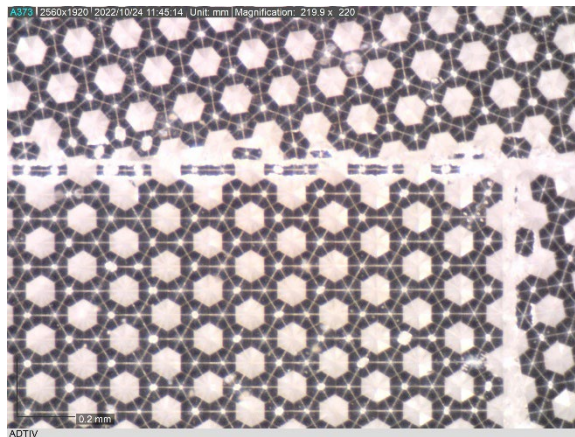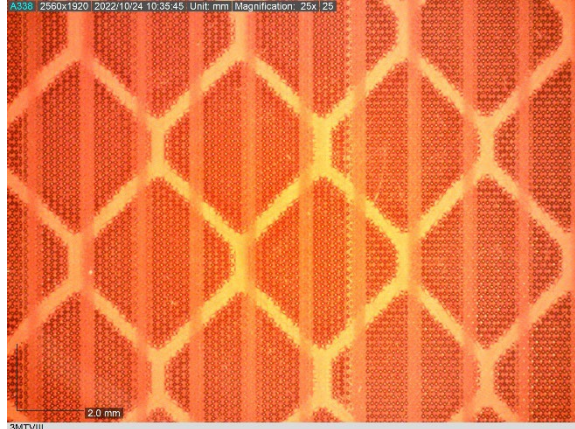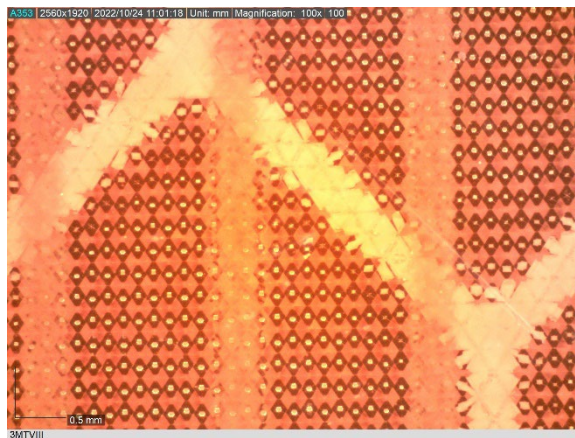(b) 100 times magnification
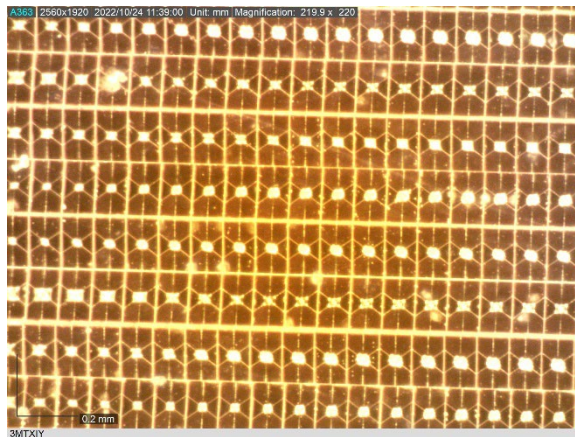
(c) 220 times magnification

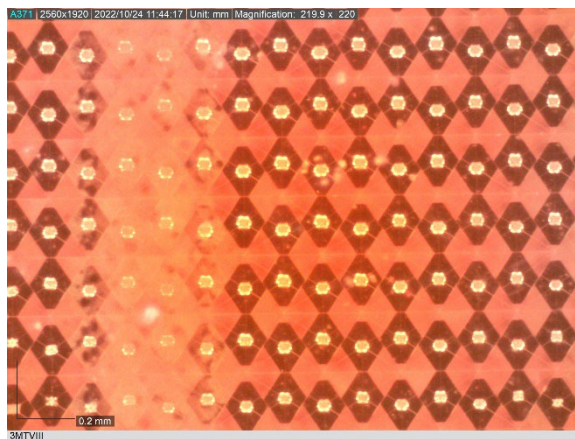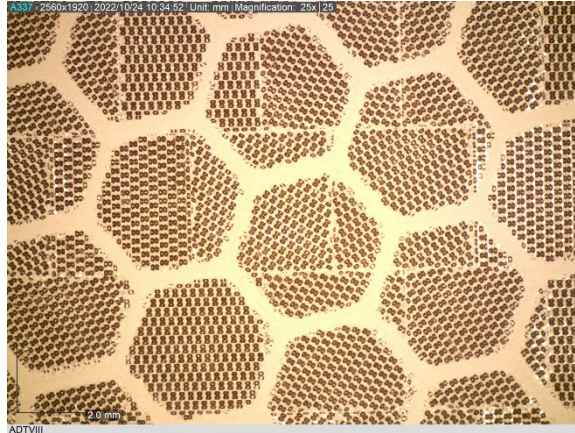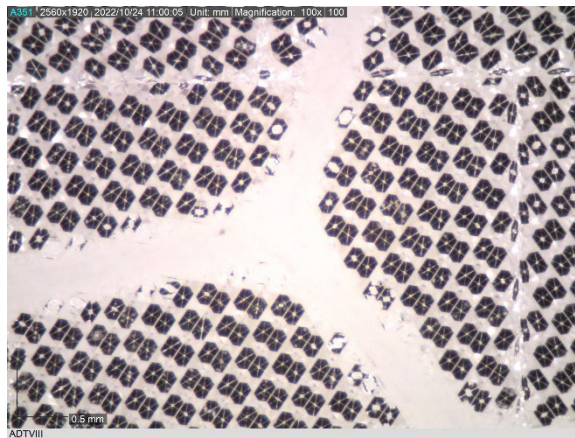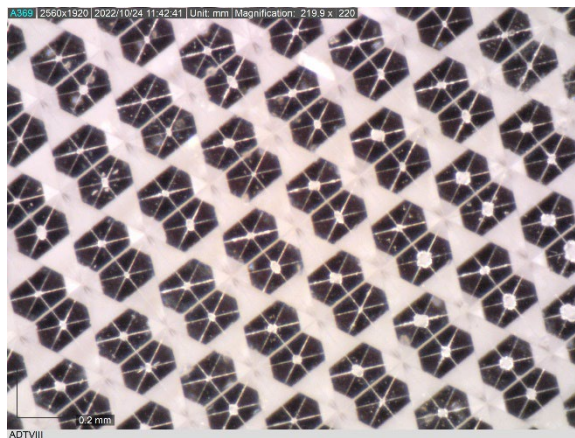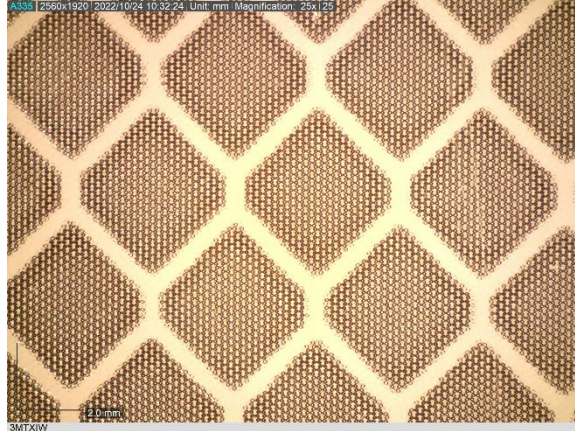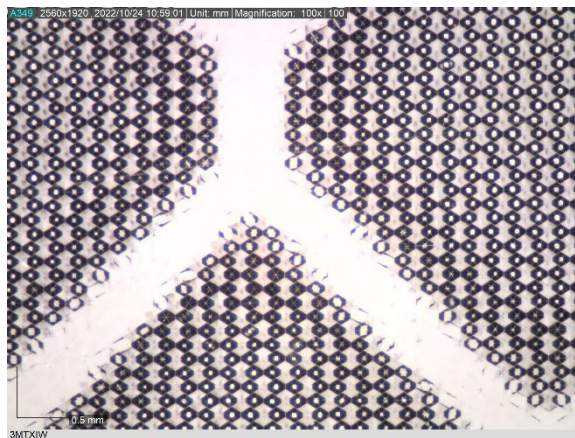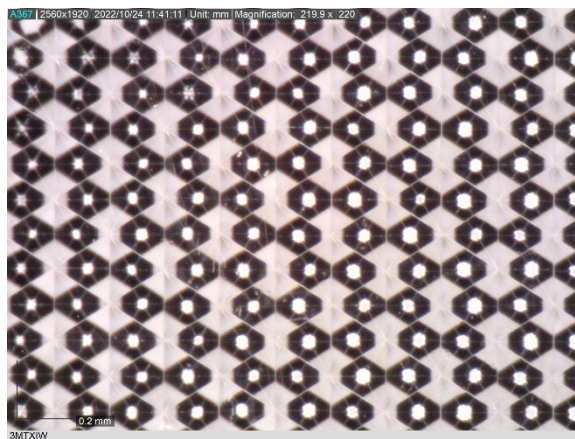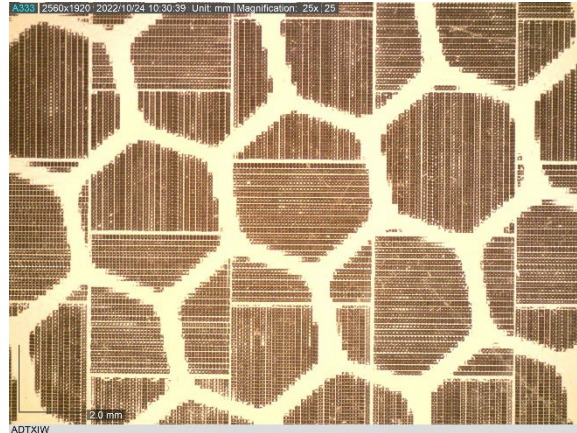*Figure 17. 3MTXIY material photos.*
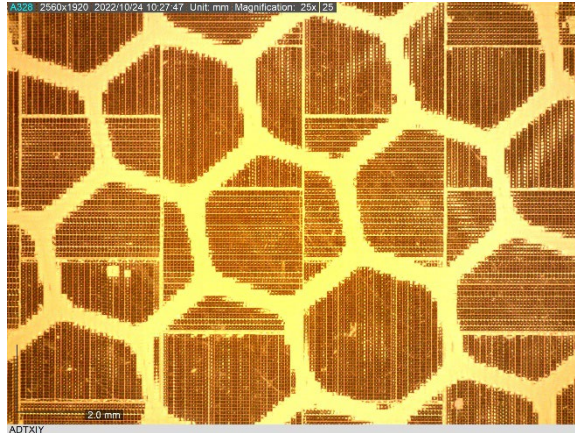
(a) 25 times magnification
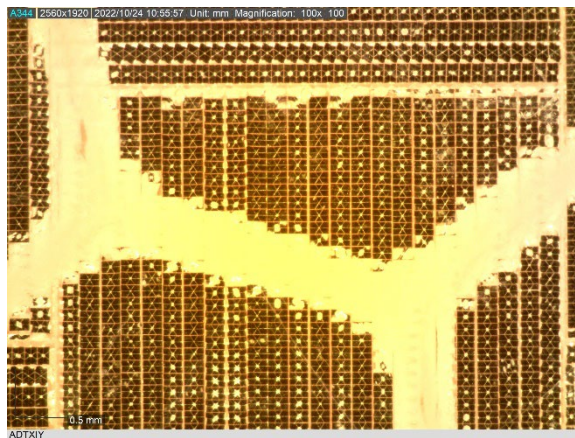
(b) 100 times magnification
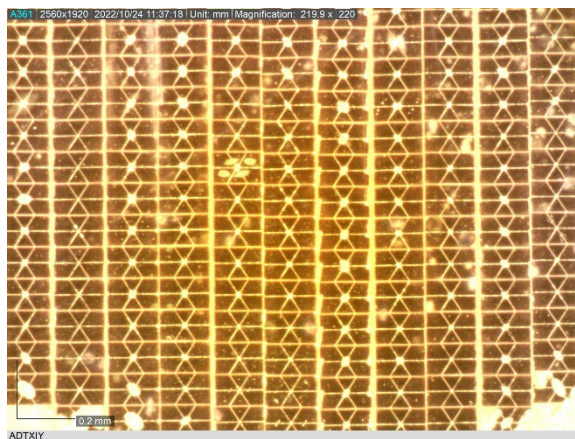
(c) 220 times magnification

Figure 18. ADTXIY material photos.

Retroreflective readings were taken using a RoadVista 922 handheld sign retroreflectometer, which is compliant with ASTM E1709 and E2540 for portable retroreflectometers [42,43]. It measures retroreflection at 0.2° and 0.5° observation angles, and for the purpose of this study, only 0.2° readings were recorded. The entrance angle is -4°. An aperture reducer was used to change the size of the aperture from 2.54 cm (1 in) to 1 cm (0.39 in). Each time the retroreflectometer was powered on, it was calibrated using the RoadVista calibration plate. To take readings, the RoadVista 922 was held flush against the specimen, the front plunger was depressed, and the trigger was pulled. The RoadVista 922 is shown in Figure 19.

Figure 19. RoadVista 922 handheld retroreflectometer

The baseline retroreflectivity of all materials was measured to determine average baseline retroreflectivity and its variability. A square foot of each material was cut, and 100 readings were taken over the area. These measurements provided insight into the variability of readings taken on the same material using a portable retroreflectometer. ADTVIII has the highest average baseline retroreflectivity of 972 cd/lx/m^2. Both manufacturers' Type I materials have the lowest retroreflective readings, both being under 100 cd/lx/m^2. The average coefficient of variation of all materials is 4.90%. The average of the 100 readings, along with ±1 standard deviation and the coefficient of variation for each material, is plotted in Figure 20.
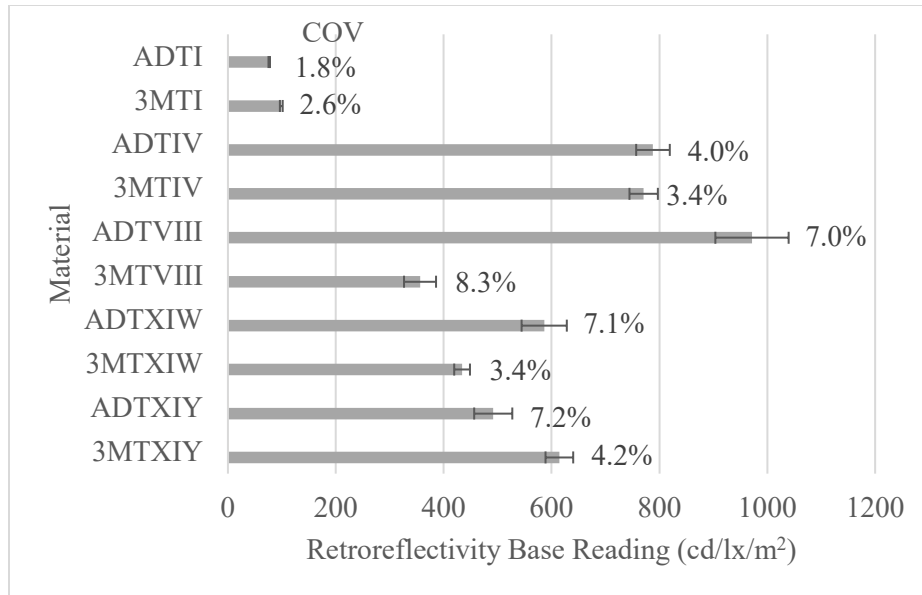
Figure 10. Variability of base retroreflectivity readings with ± 1 standard deviation and coefficients of variation.

TENSION TESTS

Tension tests were performed on 30 samples to observe the relationship between the material strain and retroreflectivity. In these tests a "dog bone" shaped specimen of RRSM was loaded in uniaxial tension to approximately 4,000 microstrain and unloaded to 0 microstrain, three times. The tests were run using an MTS Exceed Electromechanical Test System Model E42, which has a force capacity of approximately 5 kN (1,100 lb). A uniaxial resistive strain gage was bonded to the back of each specimen to measure the strain of the specimen. Strain readings were recorded using a Micro Measurements System 8,000 data acquisition system and StrainSmart software. The sample was loaded in 4.5- or 8.9-N (1- or 2-lb) increments and then held at that load, while retroreflectometer readings were taken. Four retroreflective readings were taken along the length of the specimen, the retroreflectometer averaged readings taken for each specimen, which was recorded along with the material strain and load reading at that time. Three loading and unloading cycles were executed for each specimen. Figure 21 is a photo of the tension test setup.
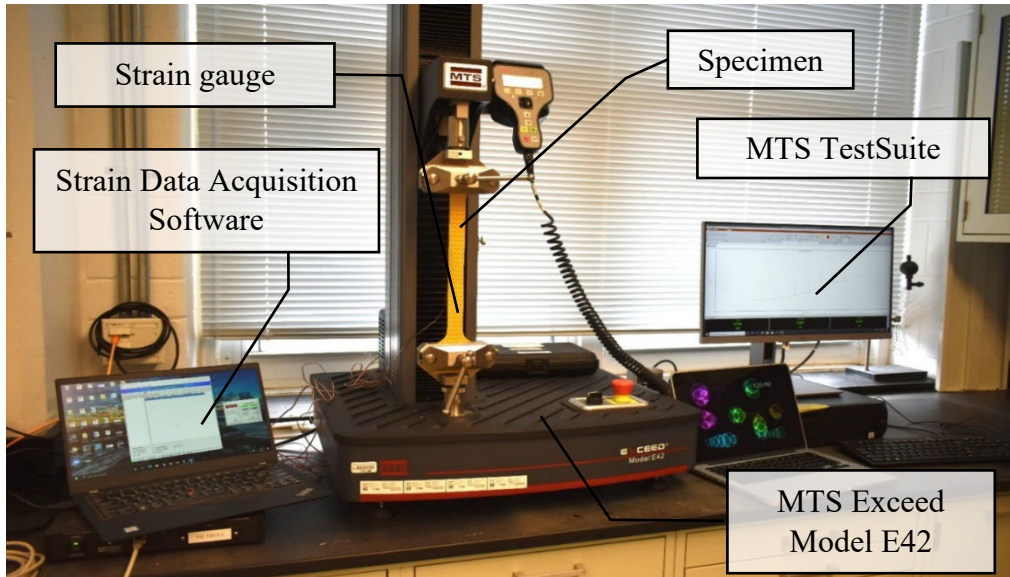
Figure 11. Test setup for investigating strain-retroreflectivity relationship.

Load was increased at a rate of 0.508 mm/min (0.02 in/min) and manually paused at every 4.5 N (1 lb) for the first loading and unloading cycle of a specimen, and every 8.9 N (2 lb) for the second and third cycles of a specimen to take retroreflective readings. Figure 22 is a schematic of the loading protocol for the tests.
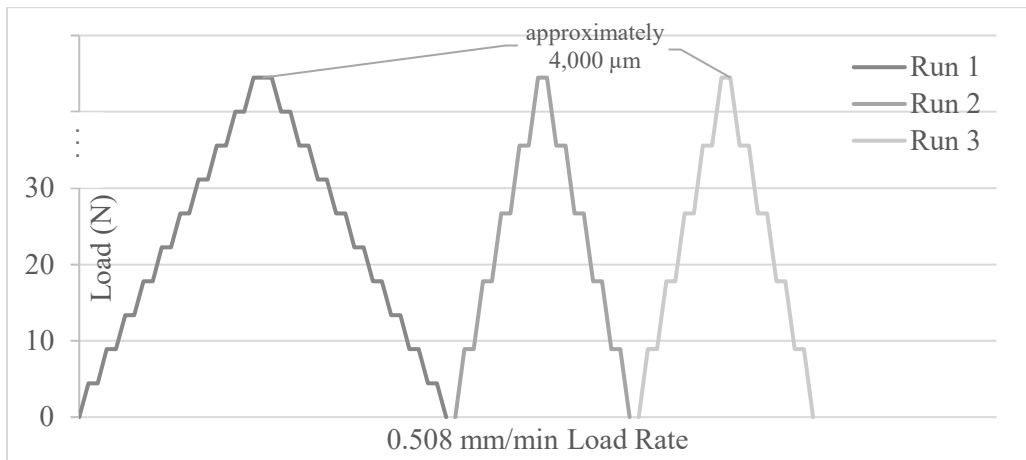
Figure 12. Loading scenario for tension tests.

Each recorded retroreflective reading was the average of four readings taken along the length of the specimen. Tension test specimen dimensions and retroreflective reading locations are shown in Figure 23.
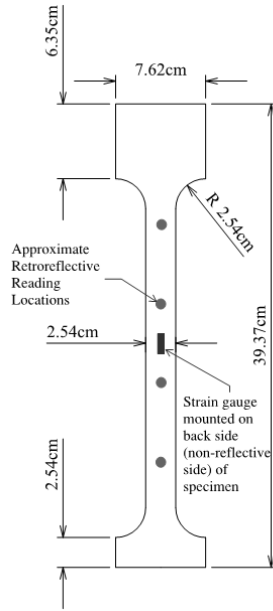
Figure 13. Specimen shape and retroreflection reading locations for tension tests.

STRENGTH TESTS

Three ultimate-strength tests were performed on each material type to determine the material tensile capacity. No strain or retroreflective readings were taken during the strength tests. The MTS Exceed Electromechanical Test System Model E42 was also used for these tests. Initially, the same specimen shape presented in Figure 4 was used for the ultimate-strength tests, but they were found to frequently fail at the ends of the gauge length. The specimen shape was modified to avoid stress concentrations toward the ends of the gauge length, and the shape used is presented in Figure 24.
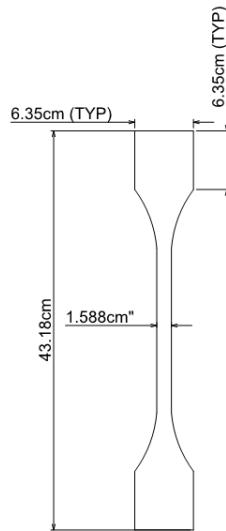
Figure 14. Specimen shape for strength tests.

The first specimen of each type was loaded at a rate of 0.508 mm/min (0.02 in/min) until it failed. The second and third specimens of each type were loaded at a rate of 1.02 mm/min (0.04 in/min) until failure. The maximum load and total extension were measured by the MTS and recorded. A caliper was used to measure the width and thickness of each specimen so that cross-sectional areas of each specimen could be calculated. The recorded values for width and thickness are the average of three measurements, taken at the bottom, middle, and top of the gauge length.

EXPOSURE TESTS

To evaluate the best way to adhere RRSM to a substrate and to determine how retroreflectivity degrades due to weathering, strips of Type XI Yellow material from both manufacturers were adhered to steel and concrete and placed outside, with a tab remaining unadhered so that specimens can be pulled off and evaluated for adhesion. For the time being, only Type XI materials were used for exposure testing, as they are the highest-grade RRSM. The initial exposure tests described herein are to determine best methods of adhesion and develop an initial understanding of how retroreflectivity and adhesion change with continued environmental exposure. Future work will include testing more types of RRSM for environmental exposure.

Various surface preparations were tested on both steel and concrete. Steel surfaces were prepared four different ways: (1) lightly wire brushing the surface, (2) wire brushing and hand sanding the surface with 40-grit sandpaper, (3) wire brushing the surface until it has a slightly shiny appearance, and (4) grinding the steel until the entire surface is shiny. RRSM samples were applied to each surface and the preparation methods were evaluated by both pulling the samples off slowly, and by quickly tearing them off, all 4 days after adhesion. From these initial tests, it was determined that the best way to adhere the material to steel would be method 3, wire brush the steel surface by hand until the surface appears slightly shiny. This method of adhesion allowed for the specimens to be adhered to the substrate with only their manufactured backing, and of the tested methods, it was the most difficult to remove these specimens, with at least a portion of the specimen remaining adhered to the steel after it was pulled off. Other methods of surface preparation did not yield the same results. When the steel surface was prepared with methods 1 and 4, the specimens tore cleanly from the steel substrate when they were slowly peeled. Method 2 resulted in the second-best adhesion but required less force to remove the specimens than method 3, and at least a portion of the RRSM did not always remain adhered to the substrate.

For adhesion to concrete, a similar application test was performed. The concrete surface was prepared two ways: by (1) wire brushing the surface by hand and by (2) wire brushing the surface by hand and then skim coating it with a two-part JB Weld ClearWeld Professional Grade Epoxy, which has a strength of 3,900 psi. For the specimens adhered using epoxy, the epoxy was spread over the surface of the concrete and allowed to set for an hour before the RRSM specimens were applied. Both methods performed well, with the RRSM adhering slightly better to the concrete surfaces that were coated with epoxy. For both methods of adhesion to a concrete substrate, the specimens that were quickly ripped off remained at least partially adhered to the concrete, but when the RRSM was pulled off slowly, the specimens adhered using method 1 were able to be cleanly removed from the substrate, while those adhered with method 2 remained at least partially adhered to the substrate.

Eighteen samples of each manufacturer's material were adhered to the steel and concrete surfaces in May 2021 using the preferred surface preparation procedures and left outside in Newark, DE. To determine how the adhesion and retroreflectivity of these specimens are affected by environmental exposure, tests will be performed at 3, 6, 12 and 24 months. At each test, three specimens of each manufacturer on each substrate will be removed from the surface to test adhesion. Two specimens will be ripped quickly and the last will be slowly pulled from the surface. This will allow for analysis of how well the RRSM remains adhered to each substrate when exposed to the environment for various periods of time. Retroreflective readings will

also be taken of the specimens that are to be removed during each of the testing time periods to determine how their retroreflectivity changes with continued exposure. Photos of the exposure test setups on steel and concrete are shown in Figure 25.
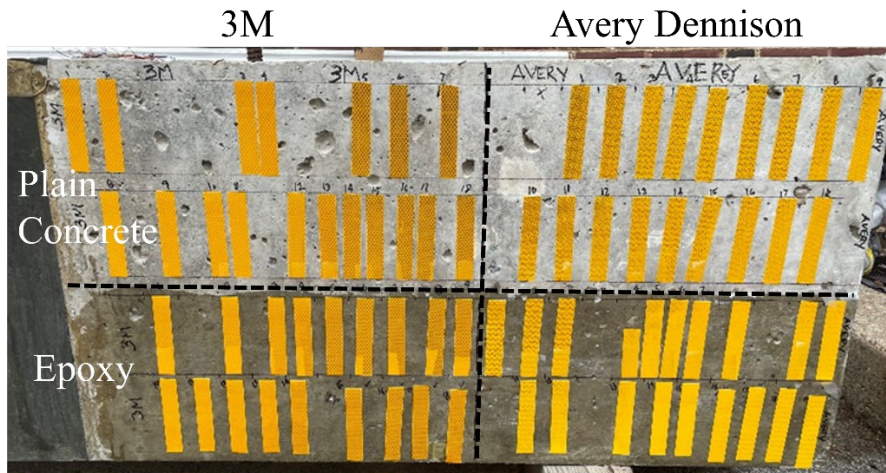
(a) Specimens on concrete

(b) Specimens on steel

Figure 15. Exposure test setup.

MICROSCOPIC EVALUATION OF RRSM DURING LOADING

To investigate why the retroreflectivity of RRSM changes with applied load, samples of various RRSM types were subjected to loading, similar to the procedure described in the Tension Tests section of Chapter 3, while the prismatic reflecting layer was evaluated at approximately 25 times magnification using a DinoLite model AM73915MZT handheld microscope. A photo of the test setup is shown in Figure 26.
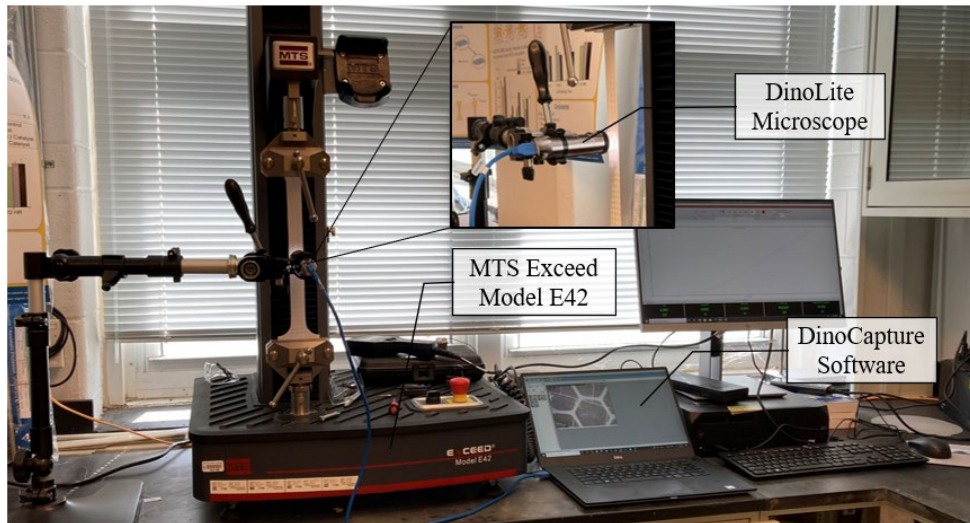
Figure 16. Microscopic evaluation test setup.

Each specimen was loaded to failure and photos were taken at 22.24-N (5-lb) intervals while a video was recorded of the test. To take the photos, loading was manually paused every 22.24 N and the DinoCapture software was used to record a photo at each interval. After each test, the recorded video was used to capture a photo of the material just prior to failure. Type IV, VIII, and XI materials manufactured by Avery Dennison have a grid pattern that can be seen using the DinoLite microscope. Using the photos taken during the tests, these grid lines were measured in the CAD program MicroStation at each interval, and the measurements were used to calculate the approximate material strains. Materials manufactured by 3M have no grid, and photos at various loading intervals were compared qualitatively to determine changes in the prismatic layer. Figure 27 shows the grid pattern of an Avery Dennison Type IV material compared to a 3M Type IV material with no grid pattern.
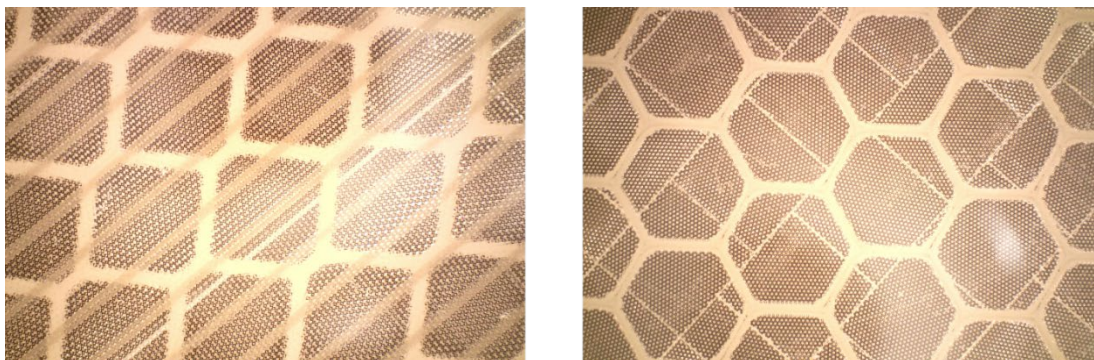
Figure 17. 3M (left) & Avery Dennison (right) Type IV RRSM depicting difference in grid pattern.

CHAPTER 4

Results

This chapter presents the results of the tests discussed in Chapter 3. Plots of each material's retroreflectivity versus strain created from data collected during the tension tests of the RRSM are used to write regression equations to determine each material's retroreflective sensitivity to strain. Results of the strength tests were used to evaluate each material's failure stress and strain. Initial environmental exposure of Type XI materials were assessed at 0, 3, and 6 months to determine their adhesion to steel and concrete and their changes in retroreflectivity. Microscopic photos of RRSMs during loading were utilized to calculate material strains that were compared to strains collected during tension tests of the materials. Results of the performed tests were used to determine which RRSMs are viable for use as passive strain sensors for structural health monitoring.

TENSION TESTS

As RRSM is loaded in tension and strain is induced in the material, its retroreflectivity tends to decrease. Certain materials' retroreflectivity decreases almost linearly as strain increases, while others have a more nonlinear relationship. Each specimen was subjected to three loading and unloading cycles. As the specimens were repeatedly loaded, particular materials maintained their initial RR-microstrain relationship, while others changed from cycle to cycle. As certain specimens were repeatedly loaded and unloaded, they did not return to their baseline retroreflectivity. Results of the tension tests were plotted as retroreflectivity (cd/lx/m²) versus microstrain (µm). For each loading and unloading cycle, linear regression fits were established, and slopes of the fits represent the retroreflective sensitivity to strain with units of RR/µm. To ascertain each of these values of slope, Equations 1–4 were used, results of which are presented in Table 2.

S_{Lj}^i = the loading slope of specimen i in cycle j

S_{Uj}^i = the unloading slope of specimen i in cycle j

S^i = the slope of the regression fit to all the data for a given specimen, i

$S_{Lj} = \frac{1}{3}\sum_{i=1}^{3} S_{Lj}^i$ = average of the loading slopes of a certain material type $\qquad$ (1)

$S_{Uj} = \frac{1}{3}\sum_{i=1}^{3} S_{Uj}^i$ = average of the unloading slopes of a certain material type $\qquad$ (2)

$S_{AVE} = \frac{1}{3}\sum_{i=1}^{3} S^i$ = average of all of the loading and unloading slopes of the 3 specimens of a certain material type $\qquad$ (3)

$S_{2,3} = \frac{1}{2}\sum_{i=2}^{3} S^i$ = average of all of the 2nd and 3rd loading and unloading slopes of the 3 specimens of a certain material type $\qquad$ (4)

Of the 10 materials tested, 4 were found to have the highest sensitivity: 3MTIV, ADTIV ADTVIII, 3MTXIY, and therefore will potentially perform best as passive strain sensors for structural health

monitoring. Table 2 shows values for all sensitivity calculations as well as R^2 values of the linear regressions, which were calculated similarly to slopes, averaging the values of R^2 for all tested specimens of a given material.

Table 2. Sensitivity and R^2 of RRSM.

Variable	Material Type I 3MTI	Material Type I ADTI	Material Type IV 3MTIV	Material Type IV ADTIV	Material Type VIII 3MTVIII	Material Type VIII ADTVIII	Material Type XIW 3MTXIW	Material Type XIW ADTXIW	Material Type XIY 3MTXIY	Material Type XIY ADTXIY
S_{L1} (R^2_{L1})	-0.042	0.004	-0.071	-0.098	-0.034	-0.126	-0.043	-0.091	-0.082	-0.069
S_{L1} (R^2_{L1})	(0.707)	(0.570)	(0.928)	(0.975)	(0.918)	(0.941)	(0.972)	(0.960)	(0.936)	(0.971)
S_{U1} (R^2_{U1})	0.005	0.004	-0.063	-0.074	-0.033	-0.108	-0.042	-0.061	-0.080	-0.062
S_{U1} (R^2_{U1})	(0.657)	(0.450)	(0.923)	(0.950)	(0.907)	(0.943)	(0.967)	(0.943)	(0.949)	(0.942)
S_{L2} (R^2_{L2})	-0.005	-0.001	-0.071	-0.085	-0.030	-0.118	-0.042	-0.070	-0.081	-0.064
S_{L2} (R^2_{L2})	(0.647)	(0.080)	(0.947)	(0.978)	(0.921)	(0.949)	(0.965)	(0.947)	(0.933)	(0.966)
S_{U2} (R^2_{U2})	0.002	0.001	-0.067	-0.073	-0.026	-0.105	-0.040	-0.061	-0.081	-0.060
S_{U2} (R^2_{U2})	(0.302)	(0.042)	(0.949)	(0.966)	(0.899)	(0.939)	(0.974)	(0.941)	(0.945)	(0.940)
S_{L3} (R^2_{L3})	-0.004	-0.001	-0.070	-0.082	-0.031	-0.104	-0.043	-0.060	-0.079	-0.060
S_{L3} (R^2_{L3})	(0.522)	(0.317)	-0.957	(0.979)	(0.928)	(0.966)	(0.973)	(0.971)	(0.940)	(0.971)
S_{U3} (R^2_{U3})	-0.003	0.001	-0.062	-0.076	-0.028	-0.102	-0.036	-0.061	-0.079	-0.056
S_{U3} (R^2_{U3})	(0.259)	(0.221)	(0.937)	(0.966)	(0.945)	(0.927)	(0.960)	(0.920)	(0.956)	(0.933)
S_{AVE} (R^2_{AVE})	-0.004	-0.001	-0.067	-0.084	-0.031	-0.113	-0.042	-0.070	-0.080	-0.064
S_{AVE} (R^2_{AVE})	(0.031)	(0.010)	(0.891)	(0.868)	(0.885)	(0.909)	(0.945)	(0.795)	(0.931)	(0.928)
$S_{2,3}$ ($R^2_{2,3}$)	-0.003	0.000	-0.067	-0.082	-0.029	-0.110	-0.041	-0.065	-0.080	-0.061
$S_{2,3}$ ($R^2_{2,3}$)	(0.059)	(0.005)	(0.915)	(0.956)	(0.903)	(0.931)	(0.944)	(0.926)	(0.933)	(0.940)

3M Type I

Type I specimens are engineering-grade retroreflective sheeting materials and have the lowest values of retroreflection of all materials tested. Initially, 3M Type I (3MTI) specimens showed a somewhat linear retroreflectivity-strain relationship, but after initial loading they did not return to their baseline retroreflectivity. The average sensitivity of the first loading cycle for 3MTI was -0.042 RR/μm and the average sensitivity of the final unloading cycle was -0.003 RR/μm. The material is very inelastic, and the reflectivity changes permanently once strained. The average R^2 value for all loading and unloading cycles is 0.086, showing that there is a high level of scatter among the data. Figure 28 is a plot of the second 3MTI specimen, which is representative of how many of the Type I specimens performed. Both manufacturers' Type I materials were loaded until the material strain stopped increasing. Due to the nature of Type 1 RRSMs, their highest value of microstrain was lower than other types, frequently falling around 2,000 μm rather than the desired 4,000 μm. The plot in Figure 28 and all subsequent plots in this section show data from all three loading and unloading runs, with the data points from the first run highlighted with a dark outline. The regression line and equation for the first loading run (S) is presented on each plot along with the R^2 value for the first loading run.

Figure 18. 3MTI-2 retroreflectivity versus strain with trendline for first loading run.

Avery Dennison Type I

Avery Dennison Type I (ADTI) specimens did not show much change in retroreflectivity as load was applied. The average sensitivity for all loading cycles of all ADTI specimens was -0.0008 RR/μm. A handful of the calculated sensitivities were positive, indicating that the retroreflectivity was not decreasing as strain increased. The average R^2 value for all runs was 0.0104, indicating very low correlation to the linear trend. A linear regression line was developed for all loading and unloading cycles of ADTI specimens, and in some cases the trend of the line of best fit was that retroreflectivity increased with strain, contrary to other findings. Figure 29 is a plot of an ADTI specimen.

Figure 19. ADTI-2 retroreflectivity versus strain with trendline for first loading run.

3M Type IV

3M Type IV (3MTIV) specimens showed good linearity between retroreflectivity and strain. The average sensitivity was -0.067 RR/µm across all loading and unloading cycles of all three specimens. The average slope of the linear regression lines for all three 3MTIV specimens for the first loading cycle was calculated as -0.0707 RR/µm, and the average slope of the linear regression lines for the third unloading cycle was -0.0621 RR/µm. Of the four materials with high sensitivities, 3MTIV had the lowest retroreflective sensitivity to strain. It is evident that 3MTIV loses some retroreflectivity with repeated loading cycles. It is noteworthy that the average sensitivity of the loading and unloading cycles for all runs of all specimens and that of only the second and third runs varied by only 0.0004 RR/µm demonstrating that it is reasonable to presume the same relationship between strain and retroreflectivity for all loading cycles of 3MTIV. The second specimen of 3MTIV had the least amount of scatter about the trend line, and its plot of retroreflectivity versus strain is shown in Figure 30.
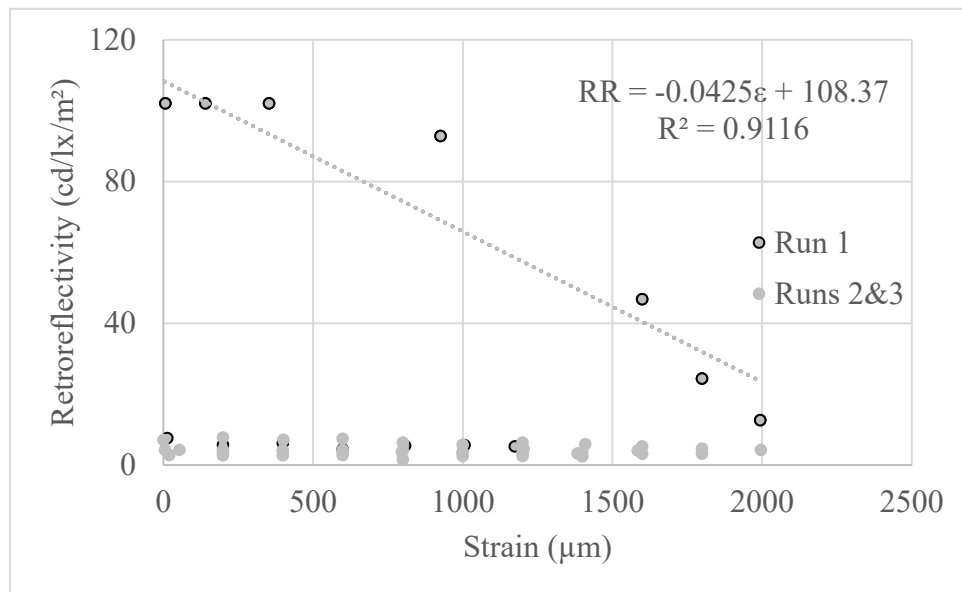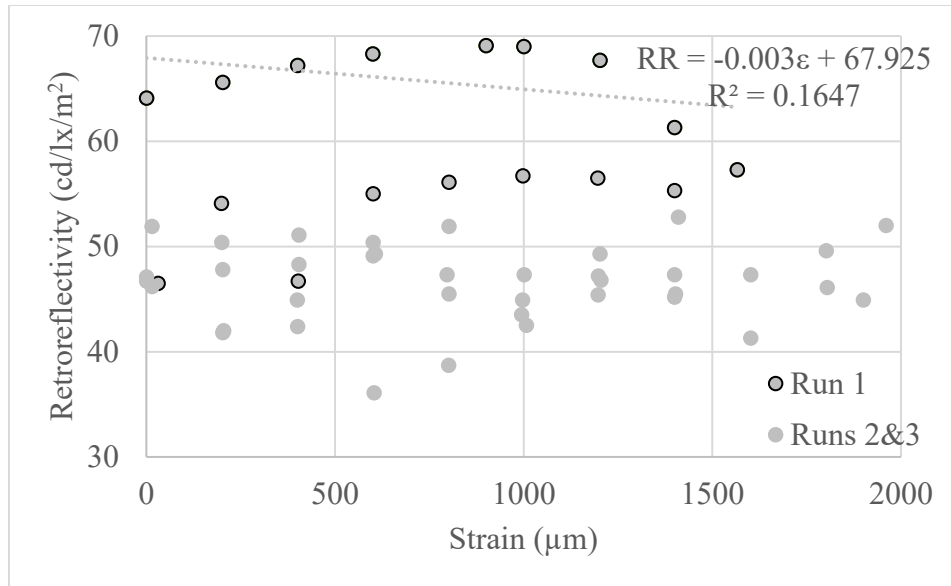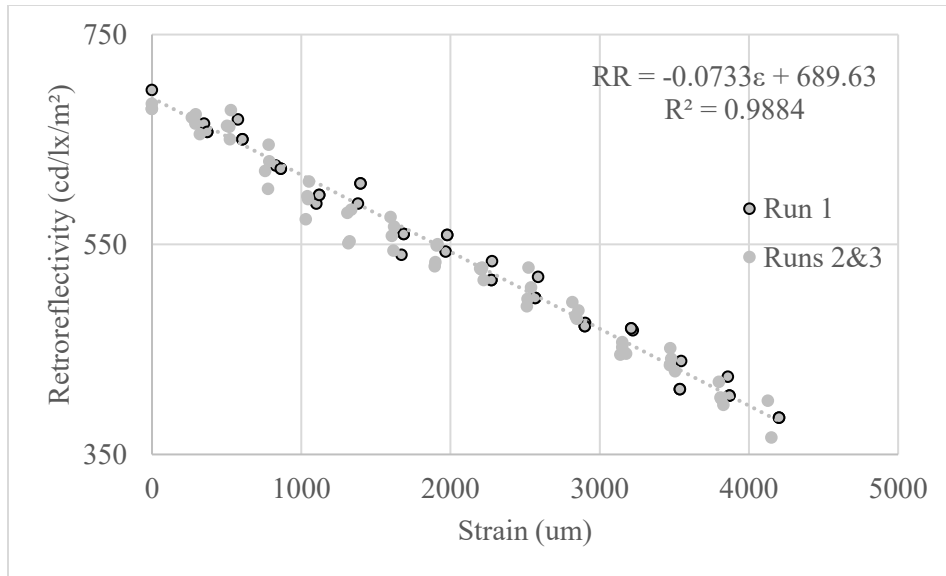
Figure 20. 3MTIV-2 retroreflectivity versus strain with trendline for first loading run.

Avery Dennison Type IV

Avery Dennison Type IV (ADTIV) specimens were shown to have moderately high retroreflective sensitivity to loading. Similar to the 3M specimens of the same material type, ADTIV specimens lost some initial retroreflectivity through repeated loading cycles. The average linear regression slope of the first loading cycle for all three specimens of ADTIV was -0.0980 RR/µm, and the average slope of all three specimens of the final unloading cycle was calculated as -0.0762 RR/µm. The difference between the average sensitivity of all cycles of all specimens and the average sensitivity of all specimens for just the second and third loading and unloading cycles was 0.0023 RR/µm, which is slightly greater than the 3MTIV materials, but it is still reasonable to adopt the same relationship between strain and retroreflectivity for all loading cycles of ADTIV. Figure 31 shows the results of one of the Avery Dennison Type IV samples.
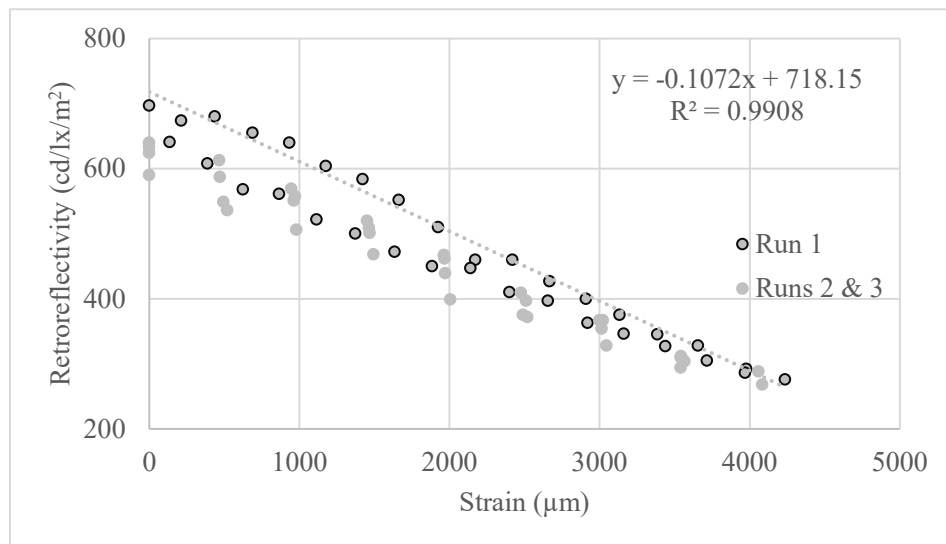
Figure 21. ADTIV-7 retroreflectivity versus strain with trendline for first loading run

3M Type VIII

Type VIII material made by 3M (3MTVIII) had a relatively low retroreflective sensitivity to strain. The average sensitivity for all loading and unloading cycles was -0.0311 RR/μm. Even though the regression slopes are not steep, they are reasonably linear. The average R^2 value for all runs was 0.8848, indicating little scatter in the data. It should be noted that the 3M Type VIII material tested was orange in color and donated by a sign shop and had been in storage for approximately 10 years. The age of the material and its color are both factors that could contribute to the fact that the retroreflective sensitivities are lower than other materials. Figure 32 is a plot of a 3MTVIII specimen.

Figure 22. 3MTVIII-1 retroreflectivity versus strain with trendline for first loading run.

Avery Dennison Type VIII

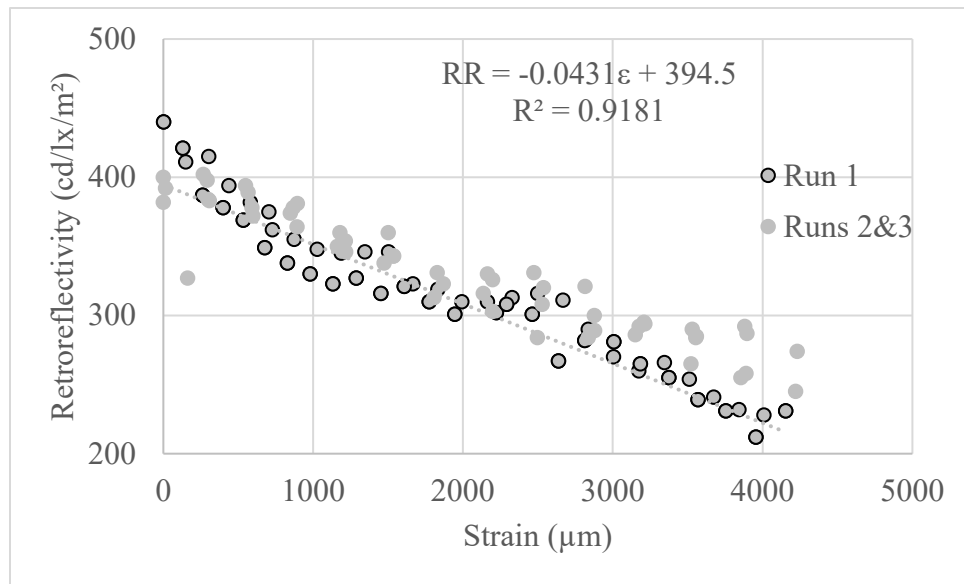Avery Dennison Type VIII (ADTVIII) materials had the highest retroreflective sensitivity to loading of all materials tested. The sensitivity of the first loading cycle was calculated to be -0.1263 RR/μm, and the sensitivity of the third unloading cycle was calculated to be -0.1018 RR/μm. Similar to both manufacturers' Type IV materials, ADTVIII loses some of its initial retroreflectivity through repeated loading cycles. Comparing the average linear regression slopes of all loading and unloading cycles for all runs to that of just the second and third runs, there is only a difference of 0.003. This demonstrates that the retroreflectivity-strain relationship developed for all runs of ADTVIII is repeatable for continued loading cycles of the material. Figure 33 is the plot of the retroreflectivity-strain relationship for a ADTVIII specimen.
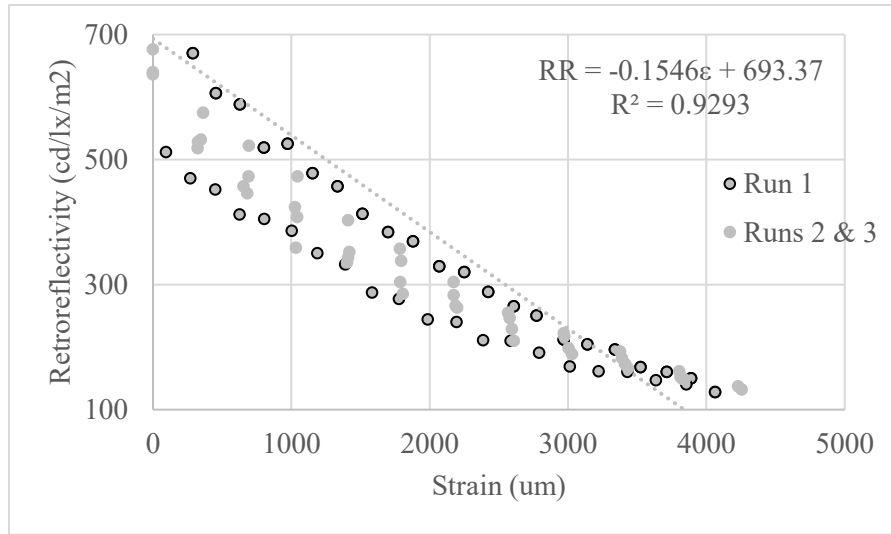
Figure 23. ADTVIII-5 retroreflectivity versus strain with trendline for first loading run.

3M Type XI White

White 3M Type XI (3MTXIW) specimens have a relatively low retroreflective sensitivity to strain. The average slope of all regression lines for all loading and unloading cycles is -0.0417 RR/μm. The initial sensitivity of the first loading run was -0.0429 RR/μm and the final unloading cycle sensitivity was -0.0361 RR/μm, a difference of 0.0068 RR/μm. The retroreflectivity of 3MTXIW does degrade somewhat with repeated loading cycles. The data show little scatter and the average R^2 value of all loading cycles of all three runs was 0.9447. Figure 34 is a plot of 3MTVIII-2.

Figure 24. 3MTVIII-2 retroreflectivity versus strain with trendline for first loading run.

Avery Dennison Type XI White

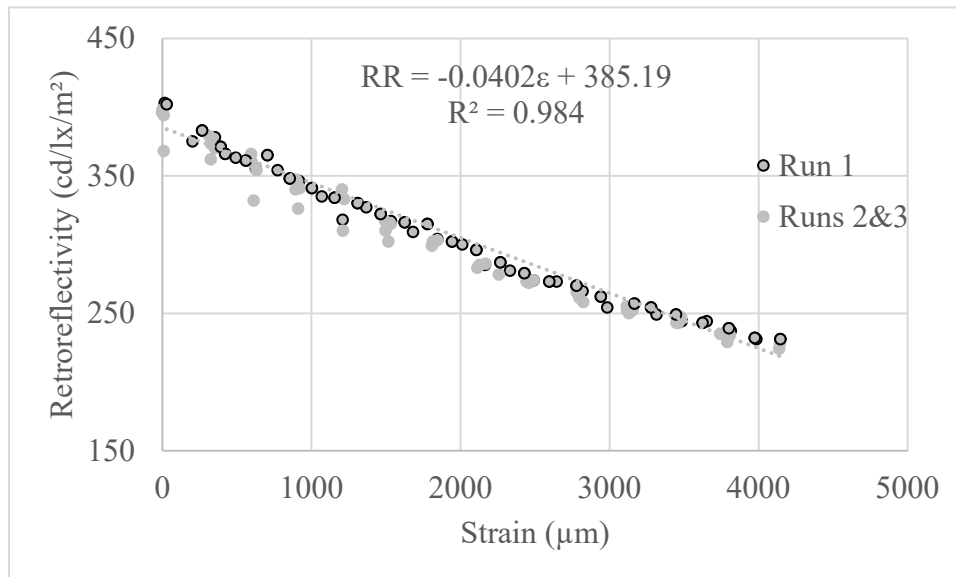Avery Dennison Type XI White (ADTXIW) specimens have a moderately high sensitivity, with an average value of -0.0697 RR/µm for all loading and unloading cycles. The sensitivity of the first loading cycle was -0.0912 RR/µm, and the final unloading cycle average sensitivity was -0.0609, showing that ADTXIW retroreflectivity greatly degrades with loading cycles. For this reason, white type XI Avery Dennison materials will not make viable strain sensors for structural health monitoring. The data show some variability, with an average R^2 value for all loading cycles of 0.7946. A plot of an Avery Dennison Type XI White material is shown in Figure 35.
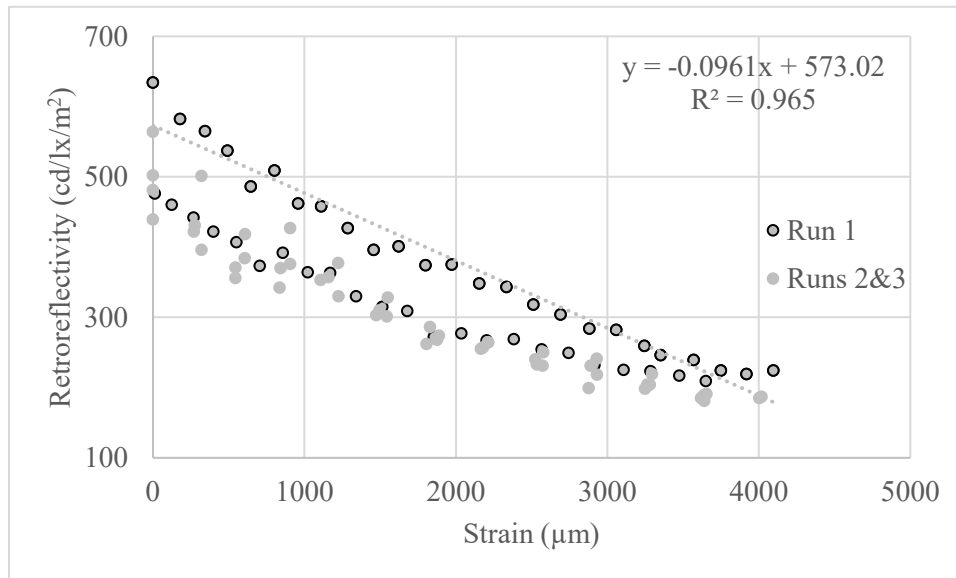
Figure 25. ADTXIW-3 retroreflectivity versus strain with trendline for first loading run.
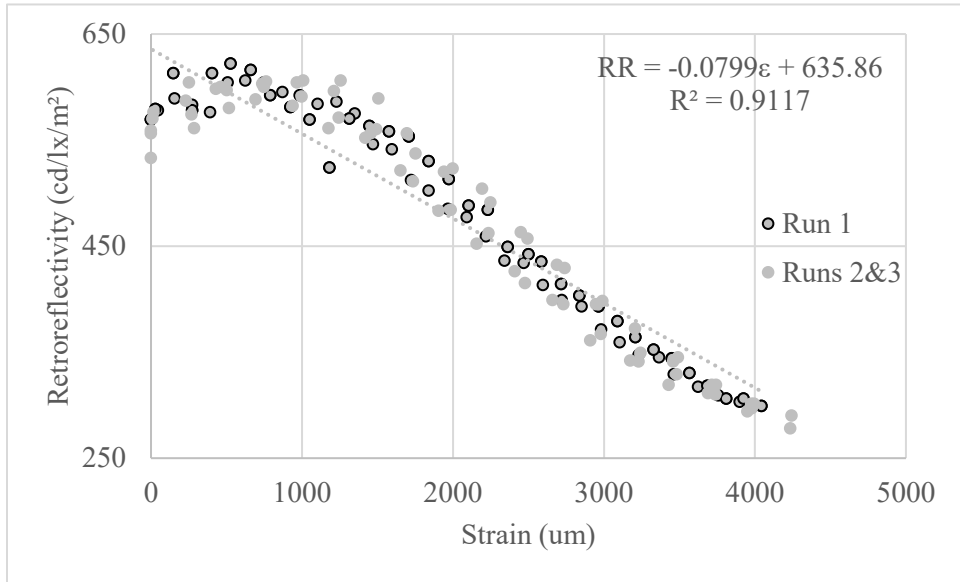
3M Type XI Yellow

3M Type XI materials that are yellow in color (3MTXIY) had linear regression slopes for retroreflectivity versus strain that were moderately high. 3MTXIY had an R^2 value of 0.931 for all loading and unloading cycles. Through plotting the data for 3MTXIY, it became apparent that retroreflectivity remained nearly constant for approximately the first 1,000 microstrain to which the specimen was subjected, and then the retroreflectivity-strain relationship became considerably more linear with increased loading. The average sensitivity of the first loading cycle was calculated as -0.0819 RR/µm and for the third unloading cycle, it was calculated as -0.0794 RR/µm, showing that the degradation in retroreflectivity through repeated loading cycles for 3MTXIY was almost negligible. Retroreflectivity versus strain for 3MTXIY specimen three is shown in Figure 36.

Figure 26. 3MTXIY-3 retroreflectivity versus strain with trendline for first loading run.

Avery Dennison Type XI Yellow

Avery Dennison Yellow Type XI (ADTXIY) material has a moderate retroreflective sensitivity to material strain. Initial loading sensitivity was -0.0694 RR/µm and final unloading sensitivity was -0.0561 RR/µm, showing that ADTXIY does lose some retroreflectivity through repeated loading cycles that it does not regain. Unlike 3M materials of the same type, Avery Dennison Type XI specimens had a relatively linear retroreflective response to material strain for the entire 4,000 microstrain range to which the specimens were subjected. The data show little scatter, with an average R^2 value for all loading cycles of 0.9275. A plot of an ADTXIY specimen is shown in Figure 37.

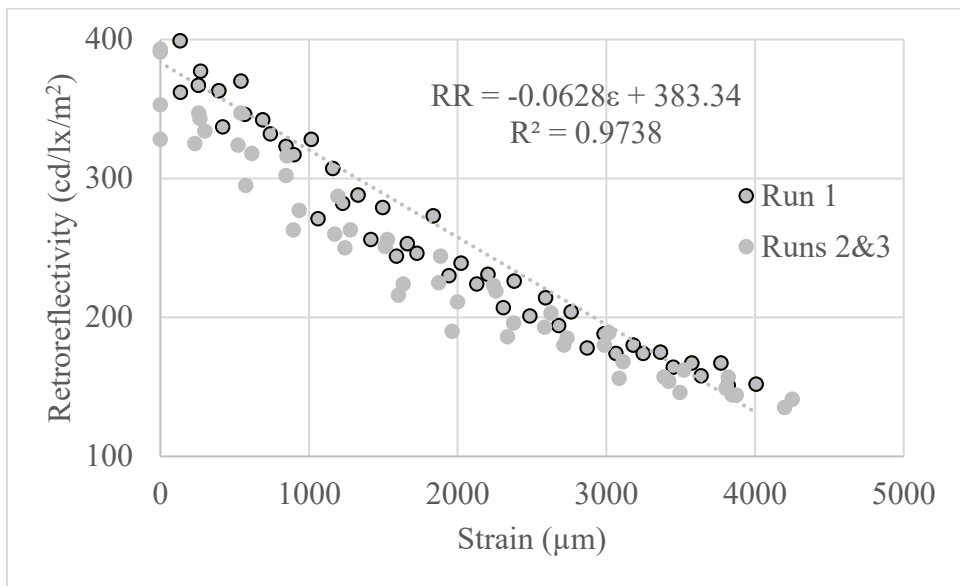***Figure 27. ADTXIY-2 retroreflectivity versus strain with trendline for first loading run.***

Presented in Figure 38(a) are data from all loading and unloading cycles of all three of the 3M materials plotted together; a similar plot of the Avery Dennison materials is shown in Figure 38(b).
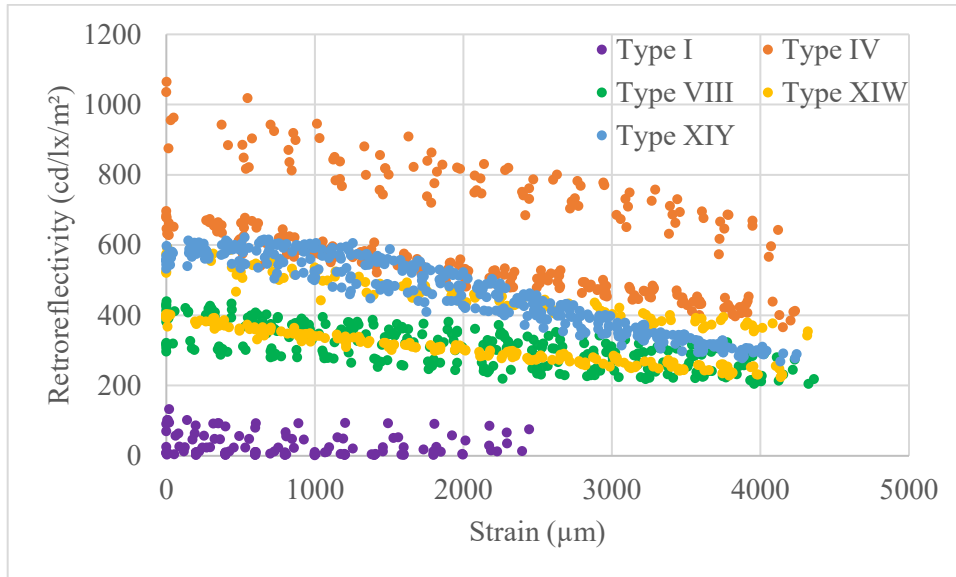
(a) All 3M RRSM Types RR-μm relationships
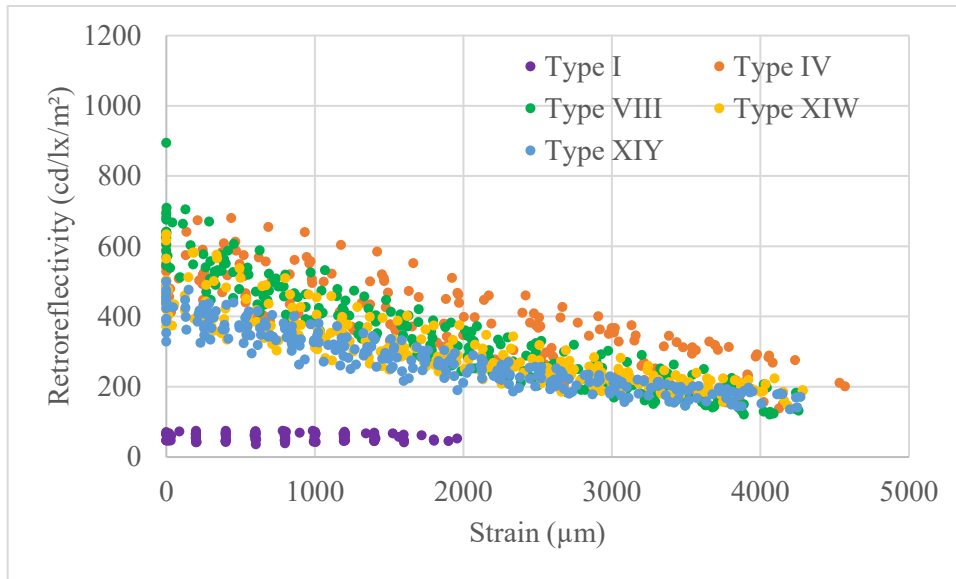
(b) All Avery Dennison RRSM Types RR-μm relationships

Figure 28. RR-μm relationships of all specimens.

STRENGTH TESTS

Results of the strength tests were used to determine RRSM properties. Failure stress in megapascals (MPa) was calculated as the maximum load recorded divided by the cross-sectional area of the specimen. Failure strain was calculated as the materials extension divided by the gauge length of the specimen. Figure 39 plots the average values of failure stress and strain as well as error of ±1 standard deviations for the RRSM tested.
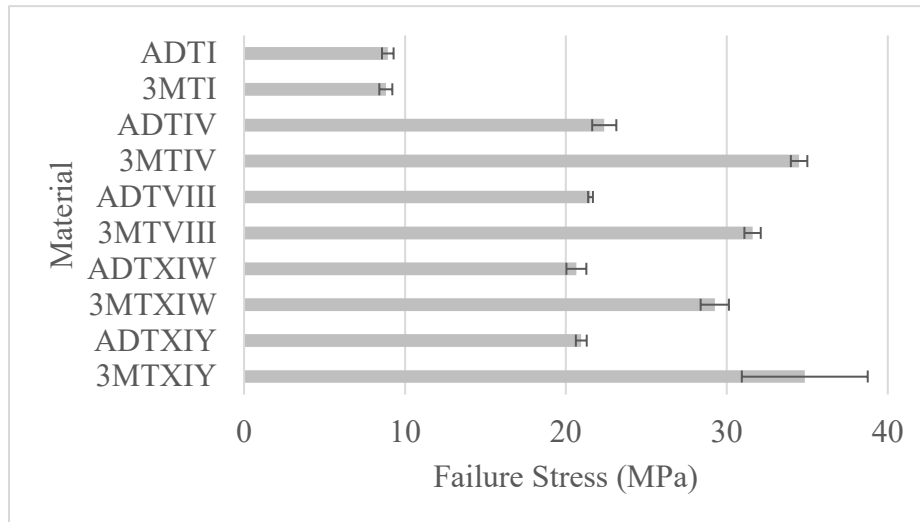
(a) Failure Stress
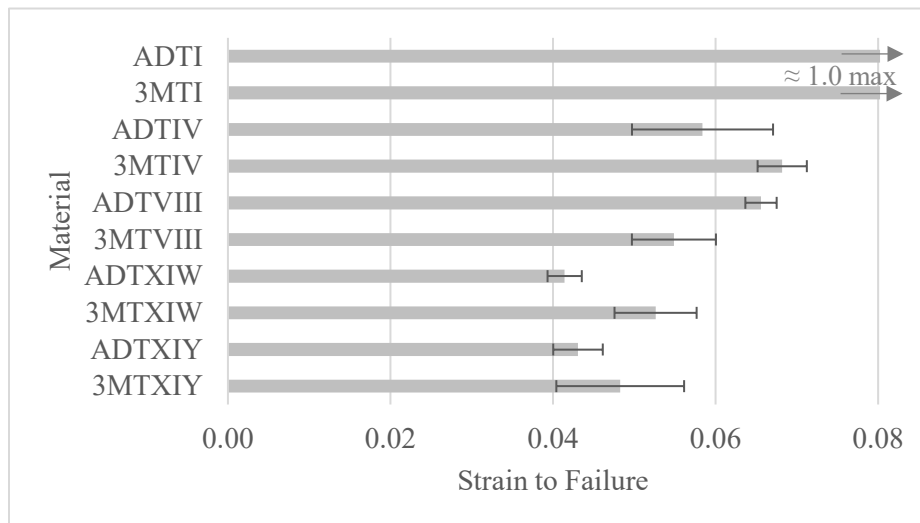
(b) Failure Strain

Figure 29. RRSM material properties determined from ultimate strength tests.

The failure stresses range from a high of 34.84 MPa for 3MTXIY to a low of 8.81 MPa for 3MTI. Excluding Type I materials, the lowest value of failure stress was 19.79 MPa for ADTXIW. Failure strains range from a high of 1.05 cm/cm for ADTI to a low of 0.04 cm/cm for ADTXIW. Excluding Type I materials, the highest value of strain to failure was 0.07 cm/cm for 3MTIV. Tensile capacities of both manufacturers' Type I materials were significantly lower than any other type, which is expected due to

their lower material grade. Type I materials are easily deformable and have high values of extension. All other materials have relatively comparable values of failure stress and strain. The results of the ultimate strength tests show that RRSM has stress and strain properties that will allow for it to be used as a passive strain sensor for structural health monitoring because the material is able to withstand very high levels of strain before breaking.

EXPOSURE TESTS

Strips of RRSM that had been previously adhered to steel and concrete surfaces, as specified in Chapter 3, were periodically evaluated for retroreflective degradation and changes in adhesion due to continued environmental exposure. Pull-off tests were performed at 3 and 6 months and retroreflective readings were taken if there was access to the retroreflectometer at those times. Similar tests were also performed at 12 and 24 months. During each of these tests, three strips of RRSM were pulled off, 2 slowly and 1 quickly, to determine their adhesion. Figure 40 shows a photo of the third 3M specimen being pulled off slowly during the 6-month adhesion tests.


Figure 30. 3M specimen adhered to steel 6-month adhesion pull-off test.

Overall, the specimens remained well adhered to the substrates. The specimens were able to be removed from the concrete and steel specimens either entirely or in part when they were slowly pulled from the surface. Specimens adhered to concrete without epoxy were easiest to remove when slowly pulled, with either the entire specimen cleanly coming off the substrate or the reflective material separating from the backing and being fully removed. Specimens pulled slowly from the epoxy-coated concrete frequently ripped and remained partially adhered to the concrete. The reflective layer and the backing of the steel-mounted specimens that were slowly pulled from the substrate separated with portions of the specimens remaining fully adhered to the steel. One of the samples mounted to the steel substrate was able to be fully pulled off at the 3-month test.

Other specimens were ripped quickly from the substrate, and those adhered to concrete without epoxy were either able to be cleanly removed or all the reflective material separated from the backing and was removed. For specimens where an epoxy skim coating was used on the concrete substrate, the majority of the RRSM strips remained adhered. When specimens mounted to steel were pulled very quickly, the majority of the specimens tore near the top of the adhered section and the specimen remained largely adhered to the substrate. Figure 41 shows specimens adhered to substrates that were either partially or entirely removed during the exposure to adhesion testing. Figure 41(a) shows the location of specimens that were adhered to bare concrete. The backing of the two specimens that were pulled quickly from the bare concrete substrate remained partially adhered, and one that was slowly pulled and came off cleanly.

Figure 41(b) depicts specimens adhered to an epoxy-coated concrete substrate where the reflective material came partially or entirely off, and the backing material remained partially adhered. Figure 41(c) shows specimens adhered to concrete that were separated near the unadhered tab with a portion of the reflective layer removed.
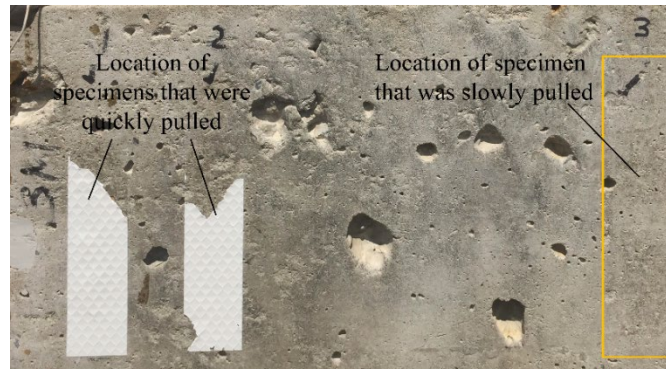
(a) Bare concrete specimens

(b) Epoxy coated concrete specimens
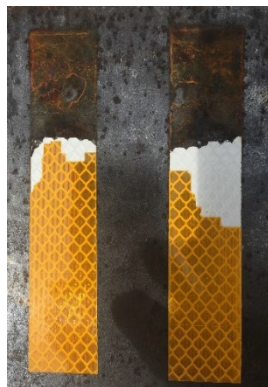
(c) Steel specimens

Figure 31. Environmental exposure specimens after attempted removal from substrate.

From the readings that were taken during the 0-, 3-, and 6-month tests, the retroreflectivity did change, some of which can be attributed to RRSM's inherent variability as discussed in Chapter 3. For many of the samples, the retroreflective readings fell within one standard deviation of the average baseline reading

for that material, showing that degradation due to weathering in this time period is negligible, and the changes in retroreflectivity that were recorded can be attributed to their baseline variability. There are specimens that had a greater change in retroreflectivity, particularly for the specimens manufactured by 3M after 6 months of exposure. These average retroreflective readings mostly differed from the initial readings by more than one standard deviation, as calculated for the baseline variability of 3MTIXY, showing that after 6 months of exposure, the material's retroreflectivity degrades.

MICROSCOPIC EVALUATION OF RRSM DURING LOADING

It is theorized that as the RRSM is loaded, the reflecting prisms themselves strain, thus resulting in the change in retroreflectivity with applied load. The four materials with the highest retroreflective sensitivity to strain, as stated previously, were loaded to failure while their prismatic reflecting layer was visually examined using a DinoLite microscope. Loading was manually paused at every 5 lb. Videos of the tests were recorded using the DinoLite microscope software, DinoCapture 2.0. At each pause in loading, a still photo of the video was captured so that changes in the material could be evaluated.

A procedure was developed to measure the approximate strain of the Avery Dennison material from the digital images. Materials manufactured by Avery Dennison have a grid pattern that was used to estimate the strain of the material by processing images in Microstation. Vertical lines of the grid were measured at each loading interval, and the approximate microstrain of the material was calculated in accordance with Equation 5:

$$\mu m = \frac{V_{avg,i} - V_{avg,0}}{V_{avg,0}} * 10^6 \tag{5}$$

where $V_{avg,i}$ is the average value of all vertical grid measurements taken of a DinoLite photo at loading interval i, and $V_{avg,0}$ is the average value of all vertical grid measurements taken of a DinoLite photo prior to loading. The DinoLite microscope was held in a fixed position during these tests, so as the specimens were loaded, the portion of material in the field of view of the DinoLite changed, and so did the grid lines measured and used to calculate strain change from one loading interval to the next. Theoretically, all grid lines are the same length and strain the same amount, as they are all close to the center of the specimen's gauge length, though in practice, it is likely that the calculated strains using different grid lines have some error, as they may not all be straining the same amount. Figure 42 shows an ADTVIII photo with vertical grid lines measured in Microstation, which was used to calculate strain.
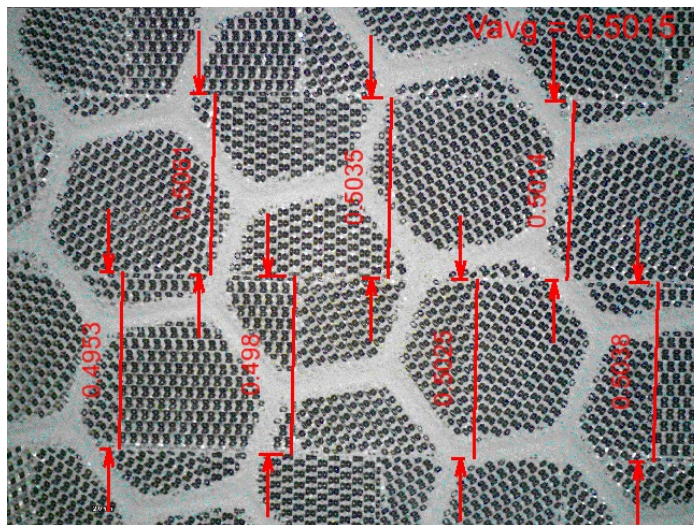
ADTVIII materials were calculated to have an average strain of 780 μm at 5 lb and 2153 μm at 10 lb from the image processing. These calculated values were compared to measured values of microstrain recorded during the tension tests presented in section 4.1: the average measured strains were 863 μm and 1,796 μm, at 5 and 10 lb, respectively from the tensile tests. Similarly, for ADTIV materials, the calculated values of microstrain using the DinoLite photos are 994 μm and 2,308 μm at 5 and 10 lb, respectively, and the measured values during the tension testes were 970 μm and 2,223 μm at 5 and 10 lb, respectively.

3MTIV and 3MTXIY specimens were also loaded to failure while evaluating the reflecting layer of the material. Strains could not be calculated due to the visual nature of the material and qualitatively, at the magnifications used, the change in the reflective prisms as the material is loaded cannot be seen. What is apparent is that the materials do not fail within prisms, but instead between prisms. In photos taken using the DinoLite, no surface fractures can be seen before failure at this magnification. A subset of photos taken during these tests can be seen in Figures 43–46.
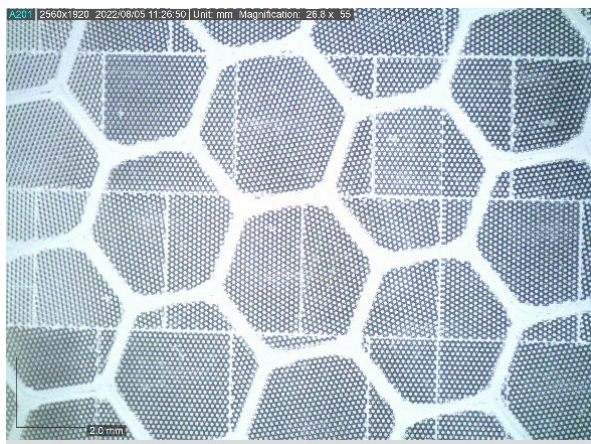
(a) ADTIV before loading
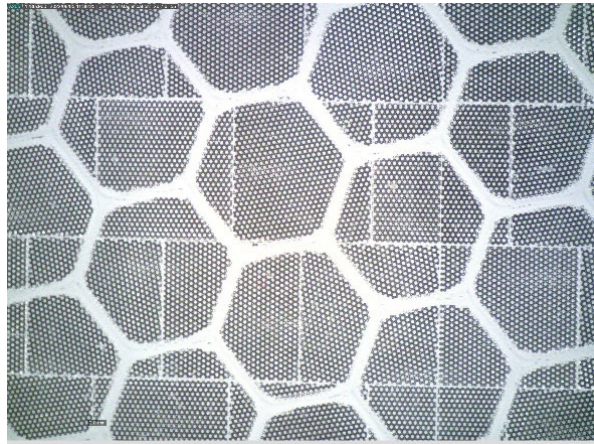
(b) ADTIV loaded to 15 lb
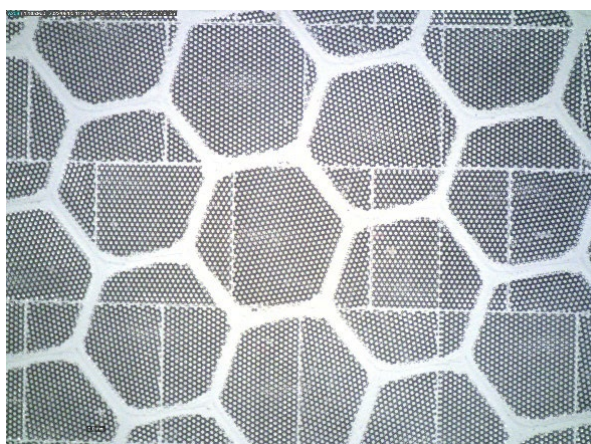
(c) ADTIV loaded to 30 lb

(d) ADTIV just before failure

Figure 33. ADTIV DinoLite photos at various values of load.
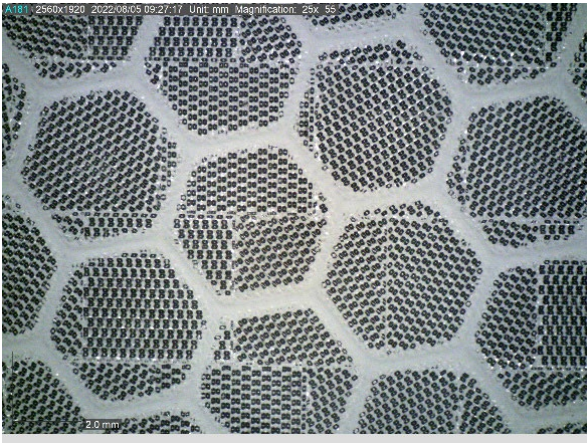
(a) ADTVIII before loading
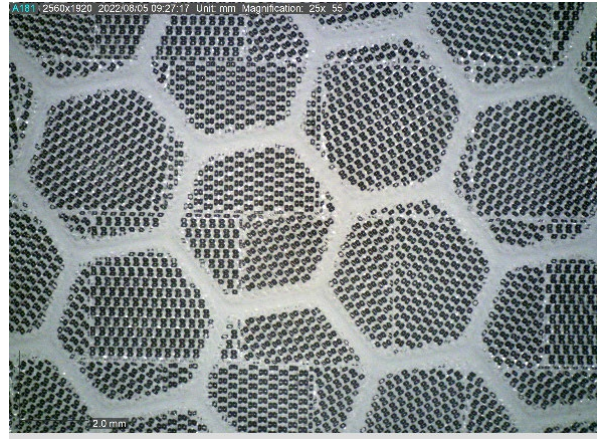
(b) ADTVIII loaded to 15 lb
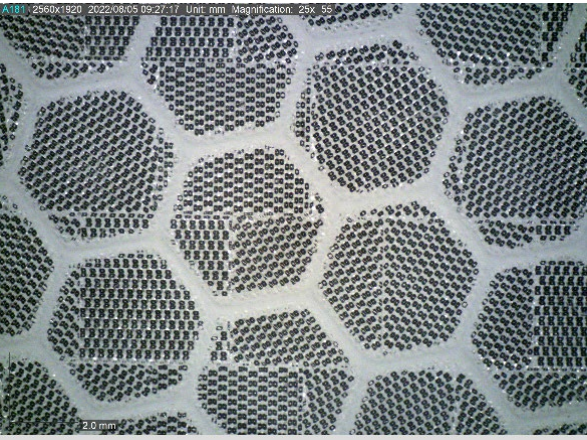
(c) ADTVIII loaded to 30 lb
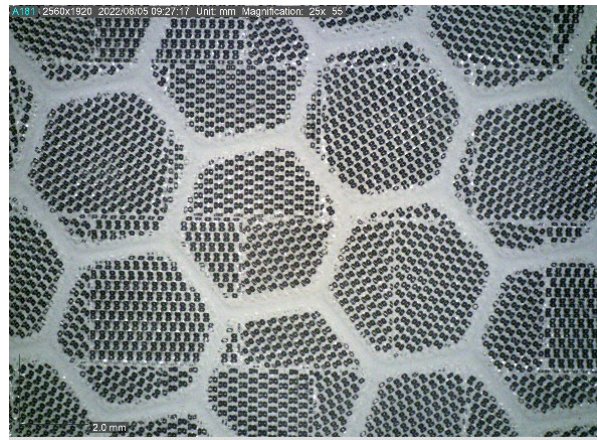
(d) ADTVIII just before failure

Figure 34. ADTVIII DinoLite photos at various values of load.
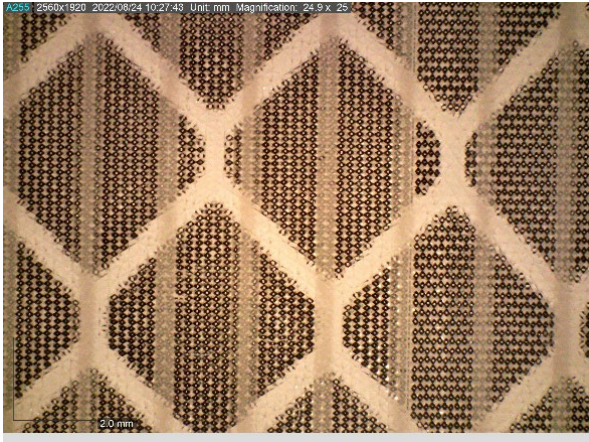
(a) 3MTIV before loading
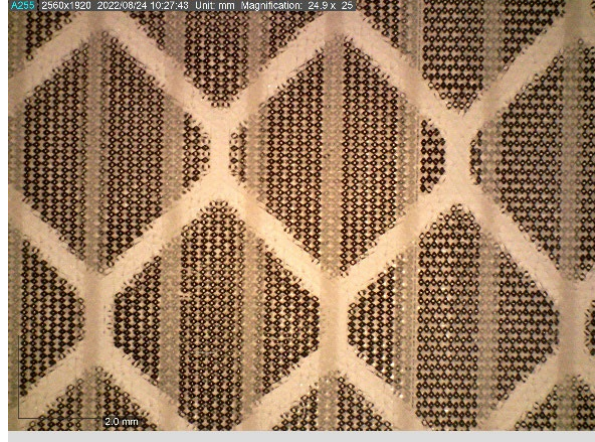
(b) 3MTIV loaded to 35 lbs
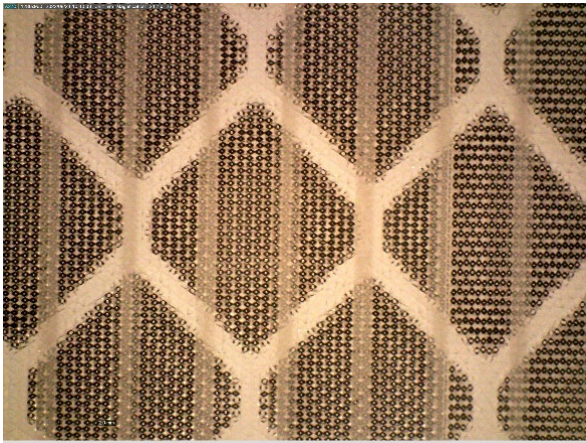
(c) 3MTIV loaded to 70 lbs
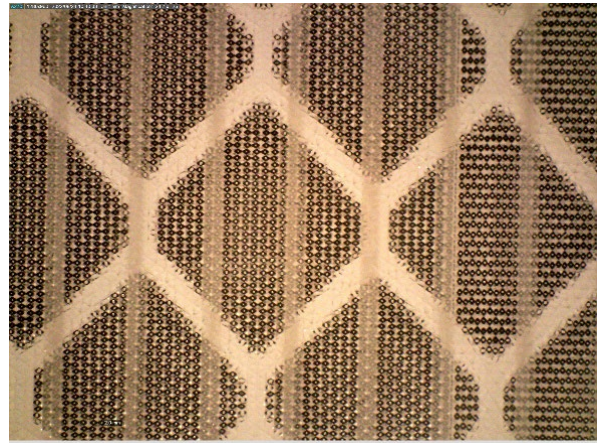
(d) 3MTIV just before failure
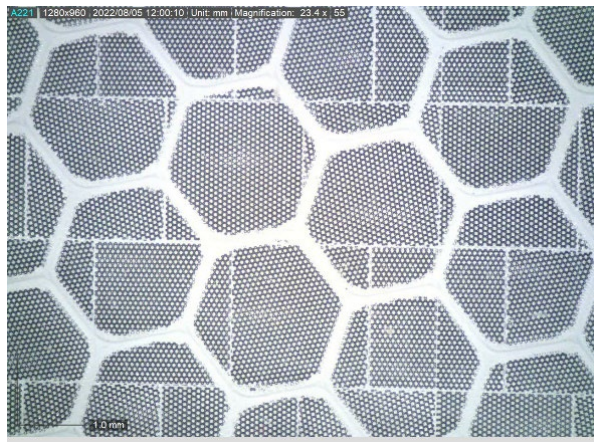
Figure 35. 3MTIV DinoLite photos at various values of load.
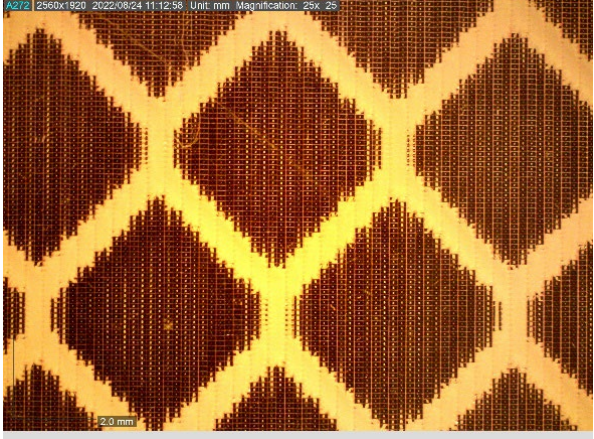
(a) 3MTXIY before loading
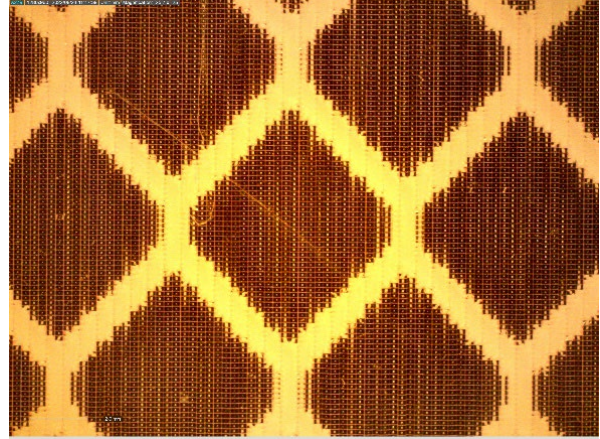
(b) 3MTXIY loaded to 35 lbs
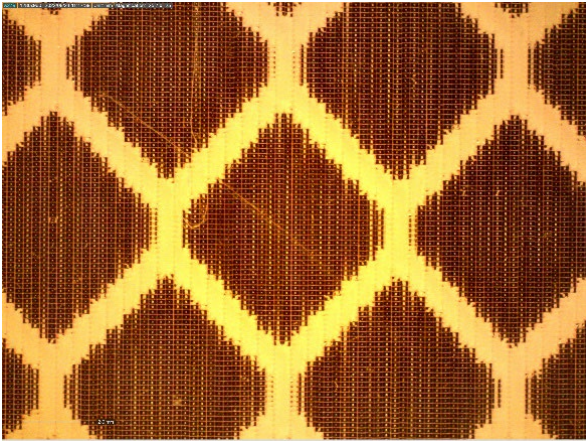
(c) 3MTXIY loaded to 70 lbs
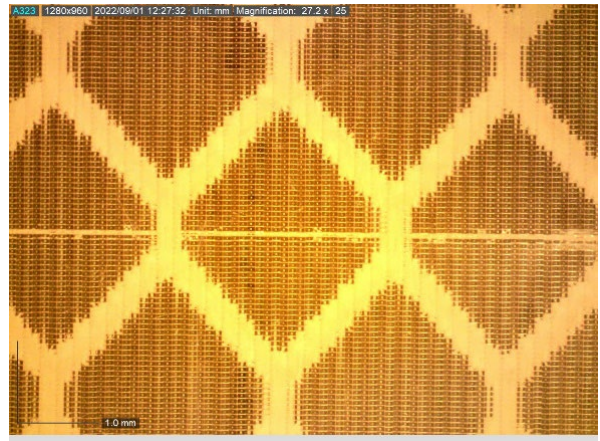
(d) 3MTXIY just before failure

Figure 36. 3MTXIY DinoLite photos at various values of load.

When the RRSM fails, it can be seen with a microscope that the failure occurs between prisms, and the prisms themselves do not fail, even though they have strained and possibly fractured. Figure 47 shows photos of failure surfaces for each of the four materials most viable for passive strain sensing.

(a) ADTIV failure surface
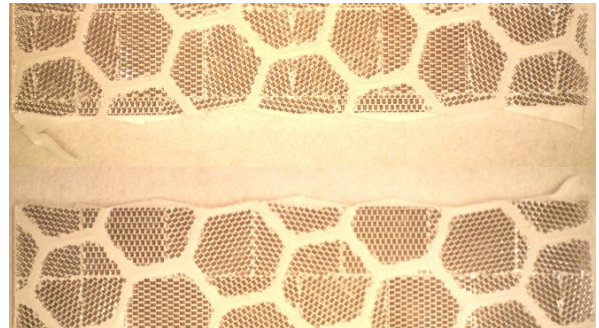
(b) ADTVIII failure surface
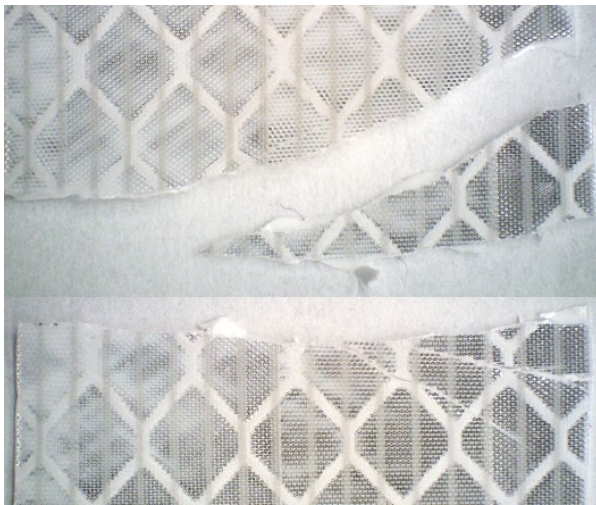
(c) 3MTIV failure surface
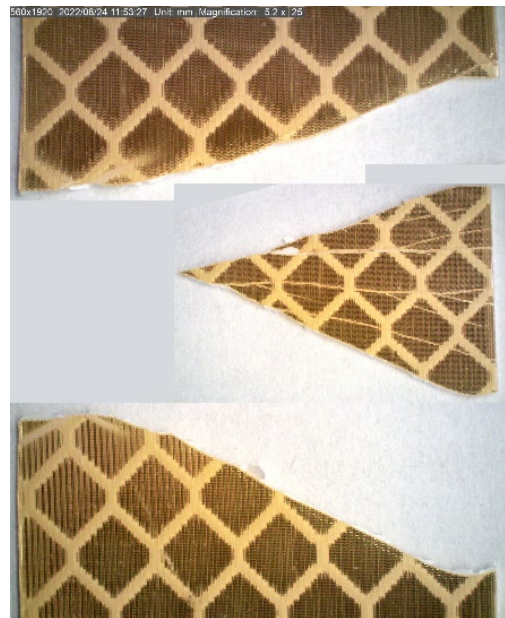
(d) 3MTXIY failure surface

Figure 37. Failure surfaces of viable RRSM types for passive strain sensing.

CHAPTER 5

Discussion

To use retroreflective sheeting materials as strain sensors for structural health monitoring, certain material characteristics are imperative. The retroreflectivity of RRSM must be sensitive to strain and degrade little with repeated load cycling, and the materials need to have high stress and strain to failure. There are other factors that affect the viability of RRSM as a strain sensor, such as adhesion to the substrate and low UV degradation. For use as a passive strain sensor for structural health monitoring, the retroreflective sensitivity of RRSM to induced strain is the most important property. The initial sensitivity of all materials is highest during the first loading cycle, before it has ever been subjected to loading, meaning that as RRSM is repeatedly loaded, its retroreflectivity degrades. To quantify the degradation of the materials for easier comparison, the average regression slope for the third loading run and third unloading run were subtracted from the average regression slope for the first loading run. These values are normalized by dividing by the slope of the first loading run. Equations for these calculations are displayed in Equations 6 and 7 and the data are presented in Table 3.

$$\Delta_L = \frac{S_{1L} - S_{3L}}{S_{1L}} \times 100 \qquad (6)$$

$$\Delta_U = \frac{S_{1L} - S_{3U}}{S_{1L}} \times 100 \qquad (7)$$

where Δ_L = percentage difference between 1st and 3rd loading run, s_{1L} = slope loading run 1 regression line, s_{3L} = slope loading run 3 regression line, Δ_U = percentage difference between 1st loading and 3rd unloading runs, s_{3U} = slope unloading run 3 regression line.

Table 3. RRSM degradation.

Variable	Sample Type I 3MTI	Sample Type I ADTI	Sample Type IV 3MTIV	Sample Type IV ADTIV	Sample Type VIII 3MTVIII	Sample Type VIII ADTVIII	Sample Type XIW 3MTXIW	Sample Type XIW ADTXIW	Sample Type XIY 3MTXIY	Sample Type XIY ADTXIY
Slope Loading Run 1 Trendline (S_{L1}) (Units: RR/µm)	-0.042	0.004	-0.071	-0.098	-0.034	-0.126	-0.043	-0.091	-0.082	-0.069
Normalized Degradation, Δ_L	91%	122%	1%	16%	11%	18%	1%	34%	4%	13%
Normalized Degradation, Δ_U	93%	77%	12%	22%	18%	19%	16%	33%	3%	19%

Referring to Table 3, the ideal RRSM strain sensor will have a high sensitivity (*S*) and low degradation with continued cycling (Δ_L, Δ_U). The retroreflectivity of Type I materials degraded significantly after the first loading cycle, and therefore they are not a good choice of material for a passive strain sensor that is subject to repeated loading cycles. 3MTIV and ADTIV have reasonably high initial sensitivities. The degradation of 3MTIV is low ($\Delta_L = 1\%, \Delta_U = 12\%$), meaning that it may be reasonable to use the same relationship of

retroreflectivity to strain for all loading cycles of 3MTIV. 3MTIV also has the highest values for failure stress and strain, excluding Type I materials. Type IV manufactured by Avery Dennison has higher values of normalized degradation, meaning that it may be beneficial to further investigate its degradation, as it is one of the most sensitive materials, making it better for use as a passive strain sensor. ADTVIII has the highest sensitivity of all the materials tested, and it also has the highest baseline retroreflectivity. The inherent variability of ADTVIII is higher than other materials, which is expected due to its higher baseline readings, and it also has relatively high values of degradation ($\Delta_L = 18\%, \Delta_U = 19\%$). 3MTVIII has low retroreflective sensitivity to strain, and even though it does not degrade much with repeated loading, it is not as sensitive as other types of RRSM. 3M and Avery Dennison Type XI White materials are very different from one another. While ADTXIW has a high initial sensitivity, with repeated loading it degrades so much ($\Delta_L = 34\%, \Delta_U = 33\%$) that it is not viable to use as a strain sensor. 3MTXIW has a moderately low sensitivity, and lower degradation ($\Delta_L = 1\%, \Delta_U = 16\%$). ADTXIY has a moderately high initial sensitivity, but relatively high values for normalized degradation. 3MTXIY has the fourth highest initial sensitivity, and very low values of initial degradation ($\Delta_L = 4\%, \Delta_U = 3\%$), making it a candidate for future use as a passive strain sensor. It is important to know the average baseline reading of the materials as well as their approximate standard deviation, so it can be determined if the changes the materials experience with repeated loading are due to inherent variability or due to loading cycles. The presented data show that while some of the variability in retroreflective readings is inherent to the material, each specimen also experienced retroreflectivity degradation with loading.

Chapter 4 presents the results for the tension tests performed to determine each material's retroreflectivity-microstrain relationship. The plots in Figures 28–38 are based on points that are average values. Each retroreflective reading displayed is the average of four readings taken along the specimen's length, and there is some amount of error expected in each of these points. The values of sensitivity calculated based on these points' linear trendlines also have some variability from sample to sample of the same material. The baseline readings taken for each material show that the variability of retroreflective readings is different for each material type and manufacturer, but their coefficients of variation are close to one another.

The RR-μm relationships of each type of RRSM were developed as linear trendlines for each loading and unloading cycle of the materials. Some materials have very tightly correlated linear relationships that can be repeated, while others do not. For example, 3MTIV has a strong linear relationship, with little retroreflective degradation, so the test can be repeated. Other materials, such as 3MTXIY, are repeatable but may be more appropriately suited to a nonlinear relationship. ADTXIW materials are suited for a linear relationship but less repeatable than other materials.

Four of the 10 materials tested stand out as the most viable passive strain sensors: 3MTIV, ADTIV, ADTVIII, and 3MTXIY. Each of these materials has a high retroreflective sensitivity to strain, high failure stress and strain, and reasonably low degradation to be able to be used for structural health monitoring.

To determine why the retroreflectivity of RRSM changes with applied load, a microscopic evaluation of the four most viable materials was performed. There is little difference between the values of measured microstrain recorded during the tension tests of the material, and the calculated values of microstrain using photos taken of the materials during loading. Qualitatively it can be determined that the prismatic layer of RRSM changes with loading and causes the retroreflective readings to change when strain is induced in the material. When closely evaluating the failure surface of specimens, it can be seen that the prisms themselves do not fracture, but instead RRSM fails between prisms. From this evaluation, it is clear that the RR changes due to the reflective layer of the RRSM straining.

CHAPTER 6

Conclusions

Ten retroreflective sheeting materials were tested to determine the relationship between their retroreflectivity and strain. Five ASTM standard RRSM types manufactured by 3M and Avery Dennison were subjected to (1) three cycles of tension tests while strain and retroreflectivity were measured, (2) strength tests to determine failure stresses and strains, (3) baseline readings to determine variability in retroreflectivity, (4) environmental exposure testing, and (5) microscopic evaluation of their reflecting layer. It is apparent that certain types of RRSM are sensitive to strain and have the potential to be used as passive strain sensors. Based on this work, the following conclusions can be drawn:

1. All of the ASTM standard RRSM tested are sensitive to strain, but to varying degrees. Some show promise for use as passive strain sensors based on their RR/strain sensitivity and level of degradation with cycling.
2. RRSM has inherent retroreflective variability and degrades with repeated loading cycles.
3. The retroreflectivity of 3MTIV, ADTIV, ADTVIII, and 3MTXIY are the most sensitive to strain, have reasonable values of degradation with repeated loading, and have relatively high values for failure stress and strain, making them the best candidates for use as sensors.
4. To ensure good adhesion of RRSM to common substrates, proper surface preparation is necessary.
5. Adhesion and retroreflectivity change as RRSM is exposed to environmental conditions.

6. Retroreflectivity of the four materials that are viable candidates for passive strain sensing changes with applied load because the prismatic reflecting layer strains, as made apparent by evaluating the materials under a DinoLite microscope.
7. Implementing RRSM in this way will allow for simple and inexpensive monitoring of various structural elements.

CHAPTER 7

Future Work

Research evaluating RRSM for use as a passive strain sensor is ongoing, and goals of the continued research include:

1. Develop a better understanding of how RRSM responds to applied load within the context of its use as a passive strain sensor.
2. Develop an analytical model that predicts retroreflectivity changes with strain.
3. Continue to characterize degradation of materials to environmental exposure.
4. Demonstrate applications of RRSM as a passive sensor in structural health monitoring of civil infrastructure.

To meet these goals, research will include three categories of testing: (1) tests to better understand the fundamental material characteristics of RRSM for strain sensing, (2) analytical/numerical modeling, and (3) application-based tests of RRSM for use as a passive strain sensor. Category 1 will include evaluating how bare RRSM responds to repeated cyclic loading and how that affects each materials RR-μm relationship. Relationships of best fit between retroreflectivity and microstrain, other than linear relationships, will also be evaluated for each material type to determine the best method of computing strain in a material based on its measure of retroreflectivity. Category 1 will also include mounting RRSM to steel specimens and cyclically loading them in tension to determine if the same relationship developed for the bare RRSM can be used when the materials are mounted to a substrate. To predict retroreflective changes with strain, future work in category 2 will first include developing a full understanding of the material makeup before, during and after loading through continued microscopic evaluation. Then 2D calculations, and later 3D calculations, can be performed to determine how the deformation relates to a change in retroreflectivity. The measurement of retroreflectivity is dependent upon the angle of incidence, the angle at which the light source hits the material. When materials are retroreflective, the angle of incidence is the same as the angle of reflection, meaning that in theory, all of the emitted light is returned to the source. The reason this is true is due to the makeup of the reflective layer of material being either metallized beads or prisms. It is theorized that as the material is strained, the angle of incidence and the angle of reflection differ due to the change in the reflective layer, changing the retroreflective reading [44]. This work may involve 2D analytical modeling, or/and 2D or 3D finite element modeling. Application-based tests in category 3 will include continued exposure testing, which will expand to include more material types and possible accelerated exposure and UV testing. This will allow for improved understanding of how RRSM will perform as strain sensors when exposed to harsh elements. In addition to strain sensing, RRSM has the potential to be used as a passive way to monitor crack growth in reinforced concrete structures. To test this, RRSM will be placed over a concrete crack and retroreflective measurements will be taken as well as crack measurements using a standard crack monitor. As the crack grows, RR readings and crack width measurements will be recorded to develop a relationship between the two for various material types. RRSM also has the potential to monitor dead load. Retroreflective readings can be taken of RRSM placed on a structure before and after dead load is applied to determine the strain induced in the material due to the load placement.

CIAMTIS
U.S. DOT Region 3 University Transportation Center

Acknowledgements

References

[1] Brownjohn, J. (2016) *Structural Health Monitoring of Civil Infrastructure* Philosophical Transactions A: Mathematical, Physical and Engineering Sciences

[2] Chang P., C., Flatau A., Liu S., C. (2003) *Review Paper: Health Monitoring in Civil Infrastructure* Sage Publications

[3] Sohn H., Farrar C. R., Hemez F., Czarnecki J. (2003) *A Review of Structural Health Monitoring Literature 1996-2001* Los Alamos National Laboratory

[4] Chen H., P., Ni Y., Q. (2018) *Introduction to Structural Health Monitoring* Structural Health Monitoring of Large Civil Engineering Infrastructure

[5] Lynch J., P., Farrar C., R., Michaels J., E. (2016) *Structural Health Monitoring: Technical Advances to Practical Implementations* IEEE

[6] Furkan M. O., Mao Q., Livadiotis S., Mazzotti M., Aktan A. E., Sumitro S. P., Bartoli I. (2017) *Multipurpose Wireless Sensors for Asset Management and Health Monitoring of Bridges* The 8th International Conference on Structural Health Monitoring of Intelligent Infrastructure

[7] Hong W., Cao Y., Wu Z. (2016) *Strain-Based Damage-Assessment Method for Bridges Under Moving Vehicular Loads Using Long-Gauge Strain Sensing* American Society of Civil Engineers

[8] Liu C., Teng J., Wu N. (2015) *A Wireless Strain Sensor Network for Structural Health Monitoring* Hindawi Publishing Corporation

[9] Thai T., T., Aubert H., Pons P., DeJean G., Tentzeris M., M., Plana R. (2013) *Novel Design of a Highly Sensitive RF Strain Transducer for Passive and Remote Sensing in Two Dimensions* IEEE Transactions on Microwave Theory and Techniques

[10] Stoffel K., Klaue K., Perren S. M. (2000) *Functional Load of Plates In Fracture Fixation in Vivo and Its Correlate in Bone Healing* Injury Volume 31

[11] Gattiker, F., Umbrecht, F., Muller, D., Neuenschwander, J., Sennhauser, U., Wendlandt, M., Hierold, C. (2007) *Novel Ultrasound Read-Out for a Wireless Implantable Passive Strain Sensor (WIPSS)* International Conference on Solid State Sensors and Actuators

[12] Liu Y., Lacher A.,. Wang G, Purekar A., Yu M. (2007) W*ireless Fiber Optic Sensor System for Strain and Pressure Measurements on a Rotor Blade* Fiber Optic Sensors and Applications

[13] Chen H., P., Ni Y., Q. (2018) *Introduction to Structural Health Monitoring* Structural Health Monitoring of Large Civil Engineering Structures

[14] Daliri A., Galehdar A., Rowe W., Ghorbani K., John S. (2011) *Utilising Microstrip Patch Antenna Strain Sensors for Structural Health Monitoring* Journal of Intelligent Material Systems and Structures

[15] Kim, S., Pakzad, S., Culler, D., Demmel, J., Fenves, G., Glaser, S., Turon, M. (2007) *Health Monitoring of Civil Infrastructures Using Wireless Sensor Networks* Proceedings of the 6th International Conference on Information Processing in Sensor Networks

[16] Shenton III H., W., Al-Khateeb H., T., Chajes, M., J., Wenczel, G. (2017) *Indian River Inlet Bridge (Part A): Description of the Bridge and the Structural Health Monitoring System* Bridge Structures – Assessment, Design and Construction

[17] Chen, Z., Zhou, X., Wang, X., Dong, L., Qian, Y. (2017) *Deployment of a Smart Structural Health Monitoring System for Long-Span Arch Bridges: A Review and a Case Study* Sensors

[18] Kaloop M., R., Elsharawy M., Abdelwahed B., Hu J., W., Kim D (2020) *Performance Assessment of Bridges Using Short-Period Structural Health Monitoring System: Sungsu Bridge Case Study* Smart Structures and Systems

[19] Jang S. D., Kang B. W., Kim J. (2012) *Frequency Selective Surface Based Passive Wireless Sensor for Structural Health Monitoring* Smart Materials and Structures

[20] Jia Y., Sun K., Agosto F. J., Quinones M. T. (2021) *Design and Characterization of a Passive Wireless Strain Sensor* Measurement Science and Technology

[21] Grayson P., E., Law W., Thompson L., D. (1998) *Not Your Father's Strain Gauge* Civil Engineering Journal

[22] Deivasigamani A., Daliri A., Wang C., H., John S. (2013) *A review of Passive Wireless Sensors for Structural Health Monitoring* Modern Applied Science

[23] Omachi M., Umemoto S., Takaki T., Matsuo K., Miyamoto N., Ishii I., Aoyama T. (2017) *Visualization of Strain and New Strain Measurement Technique* The 8th International Conference on Structural Health Monitoring of Intelligent Infrastructure

[24] DiGiampaolo E., DiCarlofelice A., Gregori A. (2017) *An RFID-Enabled Wireless Strain Gauge Sensor for Static and Dynamic Structural Monitoring* IEEE Sensors Journal

[25] Chakaravarthi G., Logakannan K., P., Philip J., Rengaswamy J., Ramachandran V., Arunachalam K (2018) *Reusable Passive Wireless RFID Sensor for Strain Measurement on Metals* IEEE Sensors Journal

[26] Watters D., G., Jayaweera P., Bahr A., J., Huesris D., L. (2002) *Design and Performance of Wireless Sensors for Structural Health Monitoring* AIP Conference Proceedings

[27] Yamaguchi I. (1988) *Advances in the Laser Speckle Strain Gauge* Optical Engineering

[28] Tan E., L., Pereles B., D., Shao R., Ong J., Ong K., G. (2008) *A Wireless, Passive Strain Sensor Based on the Harmonic Response of Magnetically Soft Materials* Smart Materials and Structures

[29] Wang Y., Tan Q., Zhang L., Li M., Fan Z., (2021) *Wireless Passive LC Temperature and Strain Dual-Parameter Sensor* Micromachines

[30] ASTM International, ASTIM D4956-19 *Standard Specification for Retroreflective Sheeting for Traffic Control*

[31] Mauri L., Battista G., Vollaro E. L., Vollaro R. L. (2018) *Retroreflective Materials for Building's Facades: Experimental Characterization and Numerical Simulations* Solar Energy

[32] Burghardt T. E., Pashkevich A., Fiolic M, Zakowska L. (2019) *Horizontal Road Markings with High Retroreflectivity: Durability, Environmental, and Financial Considerations*. Advances in Transportation Studies: An International Journal

[33] Kirk A., Hunt E. A., Brooks E. W. (2001) *Factors Affecting Sign Retroreflectivity.* Oregon Department of Transportation

[34] Saleh R., Fleyeh H., Alam M., (2022) *An Analysis of the Factors Influencing the Retroreflectivity Performance of In-Service Road Traffic Signs.* Applied Sciences

[35] Khalid M. W., Ahmed R. Yetisen A. K., Butt H. (2018) *Flexible Corner Cube Retroreflector Array for Temperature and Strain Sensing.* Royal Society of Chemistry

[36] Kostromitin K. I. (2016) *Technological Aspects of Retroreflective Sheeting Production.* International Conference on Industrial Engineering, ICIE 2016

[37] Avery Dennison Permanent Traffic Sign Sheeting, https://reflectives.averydennison.com/en/home/products/retroreflective-sheeting/permanent-traffic-sign-sheeting.html

[38] U.S. Department of Transportation Federal Highway Administration, Manual on Uniform Traffic Control Devices (MUTCD), 2009 Edition with Revision Numbers 1 and 2 Incorporated, 2012.

[39] Micro-Measurements. 2010. Document Number: 11053, Measurement of Residual Stresses by the Hole-Drilling Strain Gauge Method. *Vishay Precision Group*

[40] American Society for Testing and Materials, "Standard Test Method for Determining Residual Stresses by the Hole-Drilling Strain-Gage Method," ASTM Standard E837-20, American Society for Testing and Materials, West Conshohocken, PA (2020).

[41] 3M Road Safety Resources, Explained: ASTM Standards for Traffic Signs, https://www.3m.com/3M/en_US/road-safety-us/resources/road-transportation-safety-center-blog/full-story/~/astm-standards-for-traffic-signs/?storyid=5011bc7a-64cc-4b28-93cd-84aa9707d5dd

[42] American Society for Testing and Materials, "Standard Test Method for Measurement of Retroreflective Signs Using a Portable Retroreflectometer at a 0.2 Degree Observation Angle," ASTM Standard E1709-16, American Society for Testing and Materials, Philadelphia, PA (2022).

[43] American Society for Testing and Materials, "Standard Test Method for Measurement of Retroreflective Signs Using a Portable Retroreflectometer at a 0.5 Degree Observation Angle," ASTM Standard E2540-16, American Society for Testing and Materials, Philadelphia, PA (2022).

[44] Arnold D. (1978) *Method of Calculating Retroreflector-Array Transfer Functions.* National Aeronautics and Space Administration